

Supporting information for:

## Organoimido-Polyoxometalate Non-Linear Optical Chromophores: A Structural, Spectroscopic and Computational Study

Ahmed Al-Yasari, Nick Van Steerteghem, Hayleigh Kearns, Hani El Moll, Karen Faulds, Joseph A. Wright, Bruce S. Brunshwig, Koen Clays and John Fielden.

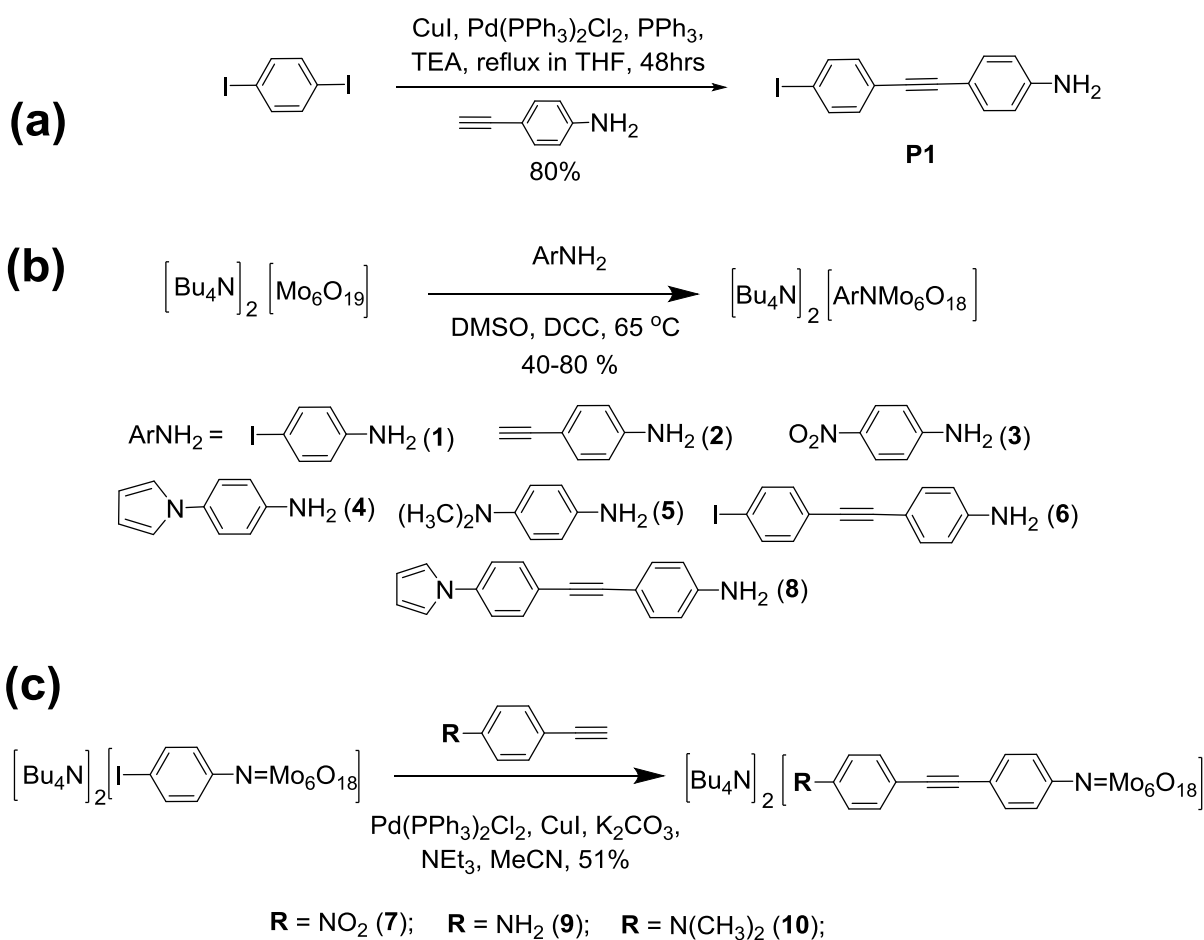
### General

**Materials and Procedures.** Tetrahydrofuran (THF), acetonitrile (MeCN) and dimethylformamide (DMF) were freshly distilled under nitrogen from an appropriate drying agent.<sup>1</sup> Dry (sure seal) dimethyl sulfoxide (DMSO) was purchased from Sigma Aldrich, and all preparations of organoimido hexamolybdate derivatives were performed under an atmosphere of dry nitrogen using standard Schlenk techniques. All other reagents and solvents were obtained as ACS grade from Sigma Aldrich, Alfa Aesar or Fisher Scientific and used as supplied. The precursors tetrabutylammonium hexamolybdate,<sup>2</sup> 4-(1H-pyrrol-1-yl)aniline,<sup>3</sup> 4-{[4-(1H-pyrrol-1-yl)phenyl]ethynyl}aniline<sup>4</sup> and 4-[(4-iodophenyl)ethynyl]aniline<sup>5</sup> were synthesized according to previously published methods, as were the hexamolybdate organoimido derivatives **1**, **4**, **8** and **9**.<sup>4</sup> Our procedure for organosilyl Keggin derivative **11** was adapted from the literature.<sup>6</sup> Nitro analogue **12** was purchased from Alfa Aesar, and **13** was synthesized according to published methods.<sup>7</sup>

**Physical Measurements.** FT-IR spectra were measured using Perkin Elmer FT-IR spectrum BX and Bruker FT-IR XSA spectrometers. <sup>1</sup>H- and <sup>13</sup>C-NMR spectra were acquired using Bruker AC 300 (300 MHz) and Bruker Ascend 500 (500 MHz) spectrometers and all shifts are quoted with respect to TMS using the solvent signals as secondary standard (s = singlet, d = doublet, t = triplet, q = quartet, sex = sextet, dt = doublet of triplets, m = multiplet). Quaternary carbon signals were not observed for the organoimido compounds even after 1064 scans of saturated d<sub>6</sub>-DMSO solutions, which gave strong signal for all other <sup>13</sup>C resonances. Elemental analyses and accurate mass spectrometry were outsourced to London Metropolitan University, and the UK National Mass Spectrometry Service at Swansea University respectively. UV-Vis spectra were obtained by using an Agilent Cary 60 UV-Vis spectrophotometer. Cyclic voltammetric measurements were carried out using Autolab PGStat 30 potentiostat/galvanostat. A single-compartment or a conventional three-electrode cell was used with a silver/silver chloride reference electrode (3M NaCl, saturated AgCl), glassy carbon or platinum working electrode and Pt wire auxiliary electrode. Acetonitrile was freshly distilled (from CaH<sub>2</sub>), [N(C<sub>4</sub>H<sub>9</sub>-*n*)<sub>4</sub>]PF<sub>6</sub>, as supplied from Fluka, and [N(C<sub>4</sub>H<sub>9</sub>-*n*)<sub>4</sub>]BF<sub>4</sub>,<sup>5</sup> were used as the supporting electrolyte. Solutions containing ca. 10<sup>-3</sup> M analyte (0.1 M electrolyte) were degassed by purging with nitrogen. All *E*<sub>1/2</sub> values were calculated from (*E*<sub>pa</sub> + *E*<sub>pc</sub>)/2 at a scan rate of 100 mV s<sup>-1</sup> and referenced to Fc/Fc<sup>+</sup>.

### Synthetic Methods

**Summary.** Our synthetic approach to the arylimido hexamolybdate derivatives, and extended iodo precursors **P1** is summarized in Scheme S1.



**Scheme S1** Synthetic approach to precursors and hexamolybdate derivatives. (a) Synthesis of 4-[(4-iodophenyl)ethynyl]aniline (**P1**).<sup>5</sup> (b) DCC-mediated synthesis of hexamolybdate derivatives. (c) Sonogashira post-functionalization used to access **7**, **9** and **10**.

**Synthesis of [(C<sub>4</sub>H<sub>9</sub>)<sub>4</sub>N]<sub>2</sub>[Mo<sub>6</sub>O<sub>18</sub>NC<sub>8</sub>H<sub>5</sub>] (**2**).** 4-ethynylaniline (0.117 g, 1 mmol), (n-Bu<sub>4</sub>N)<sub>2</sub>[Mo<sub>6</sub>O<sub>19</sub>] (1.773 g, 1.3 mmol), and DCC (1,3-dicyclohexylcarbodiimide) (0.288 g, 1.4 mmol) were heated in dry DMSO (15 mL) for 10 h at 70 °C. The colour of the solution changed to orange while it was heated. The solution was filtered into a flask containing diethyl ether (200 mL) and ethanol (50 mL) resulting in an orange precipitate. The orange precipitate was washed with ethanol and ether several times, then recrystallized twice from hot acetonitrile and washed with ethanol and diethyl ether to afford orange crystals of **2** (1.1g, 0.549 mmol, 75 %).  $\delta_{\text{H}}$  (500 MHz, CD<sub>3</sub>CN) 7.49 (d,  $J = 8.8$  Hz, 2H, H<sub>c</sub>), 7.19 (d,  $J = 8.8$  Hz, 2H, H<sub>b</sub>), 3.49 (s, 1H, H<sub>a</sub>), 3.10 (pt,  $J = 8.6$  Hz, 16H, H<sub>e</sub>), 1.61 (quin,  $J = 8.1$  Hz, 16H, H<sub>f</sub>), 1.36 (sex,  $J = 7.4$  Hz, 16H, H<sub>e</sub>), 0.97 (t,  $J = 7.4$  Hz, 24 H, H<sub>d</sub>).  $\delta_{\text{C}}$  (125 MHz, CD<sub>3</sub>CN) 133.4, 127.0, 122.3, 97.5, 83.4, 81.7, 59.4, 24.4, 20.4, 13.9. Anal. Calcd (found) % for C<sub>40</sub>H<sub>77</sub>N<sub>3</sub>O<sub>18</sub>Mo<sub>6</sub>: C, 32.82 (32.91); H, 5.30 (5.29); N, 2.87 (2.93).  $m/z = 389$  [C<sub>8</sub>H<sub>5</sub>NMo<sub>6</sub>O<sub>18</sub>]<sup>2-</sup>. FTIR: 3258 (sh); 2961 (m); 2871 (m); 1477 (s); 1378 (m); 1334 (m); 1167 (w); 1099 (vw); 976 (m); 948 (vs); 882 (w); 844 (m); 766 (vs); 650. UV-vis (MeCN)  $\lambda$ , nm ( $\epsilon$ , M<sup>-1</sup> cm<sup>-1</sup>): 264.0 (36.2 × 10<sup>3</sup>); 358.0 (27 × 10<sup>3</sup>).

**Synthesis of [(C<sub>4</sub>H<sub>9</sub>)<sub>4</sub>N]<sub>2</sub>[Mo<sub>6</sub>O<sub>20</sub>N<sub>2</sub>C<sub>6</sub>H<sub>4</sub>] (3).** A mixture of 4-nitroaniline (0.138 g, 1 mmol), (n-Bu<sub>4</sub>N)<sub>2</sub>[Mo<sub>6</sub>O<sub>19</sub>] (1.773 g, 1.3 mmol), and DCC (1,3-dicyclohexylcarbodiimide) (0.288 g, 1.4 mmol) were heated in dry DMSO (15 mL) for 10 h at 70 °C. The colour of the solution changed to orange while it was heated. The solution was filtered into a flask containing diethyl ether (200 mL) and ethanol (50 mL) resulting in a yellow precipitate. This was washed with ethanol (10 mL) and ether (10 mL) several times, before being recrystallized twice from hot acetonitrile and finally washed with ethanol (10 mL) and diethyl ether (10 mL) to afford yellow crystals of **3** (0.878g, 0.6 mmol, 60 %).  $\delta_{\text{H}}$  (500 MHz, CD<sub>3</sub>CN) 8.22 (d,  $J = 9.1$  Hz, 2H, H<sub>a</sub>), 7.34 (d,  $J = 9.1$  Hz, 2H, H<sub>b</sub>), 3.10 (pt,  $J = 8.5$  Hz, 16H, H<sub>f</sub>), 1.61 (quin,  $J = 8.0$  Hz, 16H, H<sub>c</sub>), 1.36 (sex,  $J = 7.4$  Hz, 16H, H<sub>d</sub>), 0.97 (t,  $J = 7.4$  Hz, 24 H, H<sub>e</sub>).  $\delta_{\text{C}}$  (125 MHz, CD<sub>3</sub>CN) 146.4, 126.9, 125.2, 118.4, 59.1, 24.1, 20.1, 13.6. Anal. Calcd (found) % for C<sub>38</sub>H<sub>76</sub>N<sub>4</sub>O<sub>20</sub>Mo<sub>6</sub>: C, 30.74 (30.69); H, 5.15 (5.25); N, 3.77 (3.82).  $m/z = 499.68$  [C<sub>6</sub>H<sub>4</sub>N<sub>2</sub>Mo<sub>6</sub>O<sub>20</sub>]<sup>2-</sup>. FTIR: 2961 (m); 2873 (m); 1578 (m); 1514 (m); 1480 (m); 1379 (w); 1320 (s); 1105 (w); 975 (m); 949 (vs); 857 (m); 768 (vs). UV-vis (MeCN)  $\lambda$ , nm ( $\epsilon$ , M<sup>-1</sup> cm<sup>-1</sup>): 216.0 (38.3 × 10<sup>3</sup>), 254.0 (26.3 × 10<sup>3</sup>); 287.0 (20.3 × 10<sup>3</sup>), 370.5 (30.2 × 10<sup>3</sup>).

**Synthesis of [(C<sub>4</sub>H<sub>9</sub>)<sub>4</sub>N]<sub>2</sub>[Mo<sub>6</sub>O<sub>18</sub>N<sub>2</sub>C<sub>8</sub>H<sub>10</sub>] (5).** (n-Bu<sub>4</sub>N)<sub>2</sub>[Mo<sub>6</sub>O<sub>19</sub>] (0.88 g, 0.65 mmol), 4-amino-*N,N*-dimethylaniline (0.068 g, 0.5 mmol), and DCC (1,3-dicyclohexylcarbodiimide) (0.11 g, 0.57 mmol) were added to a 50 mL flask under N<sub>2</sub> and then heated in dry DMSO (15 mL) for 10 h at 65 °C. The colour of the solution changed to black while it was heated. The solution was filtered into a flask containing diethyl ether (200 mL) and ethanol (50 mL) resulting in a black precipitate which was washed with ethanol (10 mL) and ether (10 mL) several times, then recrystallized twice from hot acetonitrile and washed with ethanol (10 mL) and diethyl ether (10 mL) to afford black crystals (0.65g, 0.43 mmol, 86 %).  $\delta_{\text{H}}$  (300 MHz, CD<sub>3</sub>CN) 7.15 (d,  $J = 9.1$  Hz, 2H, H<sub>c</sub>), 6.63 (d,  $J = 9.1$  Hz, 2H, H<sub>b</sub>), 3.09 (pt,  $J = 8.4$  Hz, 16H, H<sub>g</sub>), 3.07 (s, 6H, H<sub>a</sub>), 1.61 (quin,  $J = 8.0$  Hz, 16H, H<sub>f</sub>), 1.36 (sex,  $J = 7.3$  Hz, 16H, H<sub>e</sub>), 0.97 (t,  $J = 7.3$  Hz, 24 H, H<sub>d</sub>).  $\delta_{\text{C}}$  (125 MHz, CD<sub>3</sub>CN) 129.1, 111.9, 59.4, 40.4, 24.4, 20.4, 13.9. Anal. Calcd (found) % for C<sub>40</sub>H<sub>82</sub>N<sub>4</sub>O<sub>18</sub>Mo<sub>6</sub>: C, 32.40 (32.31); H, 5.57 (5.48); N, 3.77 (3.82).  $m/z = 498$  [C<sub>8</sub>H<sub>10</sub>N<sub>2</sub>Mo<sub>6</sub>O<sub>18</sub>]<sup>2-</sup>. FTIR: 2960 (m); 2872 (m); 1590 (s); 1511 (w); 1477 (m); 1365 (m); 1223 (w); 1176 (m); 971 (s); 944 (vs); 882 (m); 768 (vs). UV-vis (MeCN)  $\lambda$ , nm ( $\epsilon$ , M<sup>-1</sup> cm<sup>-1</sup>): 221.0 (37.5 × 10<sup>3</sup>); 258.0 (30.6 × 10<sup>3</sup>); 424.0 (32.0 × 10<sup>3</sup>).

**Synthesis of [(C<sub>4</sub>H<sub>9</sub>)<sub>4</sub>N]<sub>2</sub>[Mo<sub>6</sub>O<sub>18</sub>N<sub>2</sub>C<sub>14</sub>H<sub>8</sub>I] (6).** 4-[(4-iodophenyl)ethynyl]aniline (**P1**) (0.32 g, 1 mmol) was mixed with (n-Bu<sub>4</sub>N)<sub>2</sub>[Mo<sub>6</sub>O<sub>19</sub>] (1.773 g, 1.3 mmol), and DCC (1,3-dicyclohexylcarbodiimide) (0.237 g, 1.15 mmol) and then heated in dry DMSO (15 mL) for 10 h at 65 °C. After cooling to room temperature, the solution was filtered into a flask containing diethyl ether (200 mL) and ethanol (50 mL) and left to stand for 4 hours resulting in a red sticky precipitate. This was washed with ethanol (10 mL) and ether (10 mL) several times before being recrystallized twice from hot acetonitrile and washed with ethanol (10 mL) and diethyl ether (10 mL) to give red crystals of **6** (0.55 g, 0.32 mmol, 32 %).  $\delta_{\text{H}}$  (500 MHz, CD<sub>3</sub>CN) 7.78 (d,  $J = 8.63$  Hz, 2H), 7.55 (d,  $J = 8.63$  Hz, 2H), 7.31 (t,  $J = 8.48$  Hz, 2H), 7.23 (d,  $J = 8.48$  Hz, 2H), 3.10 (pt,  $J = 8.56$  Hz, 16H), 1.61 (quin,  $J = 8.0$  Hz, 16H, H<sub>j</sub>), 1.36 (sex,  $J = 7.41$  Hz, 16H), 0.97 (t,  $J = 7.38$  Hz, 24 H).  $\delta_{\text{C}}$  (125 MHz, CD<sub>3</sub>CN) 139, 134.4, 127.37, 123.2, 95.48, 92.3, 91, 59.6, 24.6, 20.59, 14.06. Anal. Calcd (found) % for C<sub>46</sub>H<sub>80</sub>IMo<sub>6</sub>N<sub>3</sub>O<sub>18</sub>: C, 33.16 (33.07); H, 4.84 (4.94); N, 2.52 (2.59).  $m/z = 590$  [Mo<sub>6</sub>O<sub>18</sub>N<sub>2</sub>C<sub>14</sub>H<sub>8</sub>I]<sup>2-</sup>. UV-vis (MeCN)  $\lambda$ , nm ( $\epsilon$ , M<sup>-1</sup> cm<sup>-1</sup>): 381.0 (40.0 × 10<sup>3</sup>); 298.5 (31.8 × 10<sup>3</sup>); 235.5 (31.4 × 10<sup>3</sup>)

**Synthesis of [(C<sub>4</sub>H<sub>9</sub>)<sub>4</sub>N]<sub>2</sub>[Mo<sub>6</sub>O<sub>20</sub>N<sub>2</sub>C<sub>14</sub>H<sub>8</sub>] (7).** Compound **1** (0.735 g, 0.50 mmol), ethynyl-4-nitrobenzene (0.088 g, 0.6 mmol), Pd(PPh<sub>3</sub>)<sub>2</sub>Cl<sub>2</sub> (0.007 g, 0.01 mmol), CuI (3 mg, 0.016 mmol) and K<sub>2</sub>CO<sub>3</sub> (0.500 g, 3.6 mmol) were added to a Schlenk flask which was then evacuated and backfilled with nitrogen three times. Anhydrous acetonitrile (10 mL) and dry triethylamine (0.5 mL) were then

added to the flask. After stirring at room temperature for 0.5 h under nitrogen, the reaction mixture was filtered and the filtrate was concentrated to about 2 mL before pouring into diethyl ether (200 mL) to afford a dark-red solid. This was washed successively with ethanol (10 mL) and ether (10 mL) and then recrystallized twice from (MeCN:EtOH) mixture to yield dark-red solid (0.475 g, 0.3 mmol, 60 %).  $\delta_{\text{H}}$  (300 MHz, CD<sub>3</sub>CN) 8.24 (d,  $J = 8.9$  Hz, 2H, H<sub>a</sub>), 7.75 (d,  $J = 8.9$  Hz, 2H, H<sub>b</sub>), 7.61 (d,  $J = 8.8$  Hz, 2H, H<sub>d</sub>), 7.26 (d,  $J = 8.8$  Hz, 2H, H<sub>c</sub>), 3.10 (pt,  $J = 8.6$  Hz, 16H, H<sub>h</sub>), 1.61 (quin,  $J = 8.0$  Hz, 16H, H<sub>g</sub>), 1.36 (sex,  $J = 7.4$  Hz, 16H, H<sub>f</sub>), 0.97 (t,  $J = 7.3$  Hz, 24 H, H<sub>e</sub>).  $\delta_{\text{C}}$  (125 MHz, CD<sub>3</sub>CN) 148.2, 133.3, 132.8, 130.2, 126.9, 124.5, 121.9, 109.6, 93.9, 90.8, 59.1, 24.1, 20.1, 13.6. Anal. Calcd (found) % for C<sub>46</sub>H<sub>80</sub>N<sub>4</sub>O<sub>20</sub>Mo<sub>6</sub>: C, 34.86 (34.76); H, 5.09 (5.01); N, 3.54 (3.59).  $m/z = 549.9$  [C<sub>14</sub>H<sub>8</sub>N<sub>2</sub>Mo<sub>6</sub>O<sub>20</sub>]<sup>2-</sup>, 1341.5 [(NBu<sub>4</sub>)[C<sub>14</sub>H<sub>8</sub>N<sub>2</sub>Mo<sub>6</sub>O<sub>20</sub>]]<sup>1-</sup>. FTIR: 2961 (m); 2873 (m); 2212 (m); 1592 (m); 1515 (m); 1479 (m); 1379 (w); 1338 (s); 1105 (w); 974 (m); 947 (vs); 775 (vs). UV-vis (MeCN)  $\lambda$ , nm ( $\epsilon$ , M<sup>-1</sup> cm<sup>-1</sup>): 241.0 (36.0 × 10<sup>3</sup>); 269.0 (29.9 × 10<sup>3</sup>); 389.0 (49.6 × 10<sup>3</sup>).

**Synthesis of [(C<sub>4</sub>H<sub>9</sub>)<sub>4</sub>N]<sub>2</sub>[Mo<sub>6</sub>O<sub>18</sub>N<sub>2</sub>C<sub>20</sub>H<sub>14</sub>] (10).** **1** (0.395 g, 0.25 mmol), 4-ethynyl-*N,N*-dimethylanilinenylaniline (0.0435 g, 0.3 mmol), Pd(PPh<sub>3</sub>)<sub>2</sub>Cl<sub>2</sub> (0.0035 g, 0.005 mmol), CuI (0.0015 mg, 0.0079 mmol) and K<sub>2</sub>CO<sub>3</sub> (0.25 g, 1.8 mmol) were added to a Schlenk flask which was evacuated and backfilled with nitrogen three times and then charged with anhydrous acetonitrile (10 mL) and dry triethylamine (0.5 mL). The reaction mixture was stirred at room temperature for 0.5 h under nitrogen, and then filtered and the filtrate concentrated to about 2 mL before pouring into diethyl ether to afford a dark-red solid. This was washed successively with ethanol and ether to yield dark-red solid, **10** (0.3 g, 0.189 mmol, 74 %).  $\delta_{\text{H}}$  (500 MHz, CD<sub>3</sub>CN) 7.46 (d,  $J = 8.6$  Hz, 2H, H<sub>e</sub>), 7.37 (d,  $J = 8.9$  Hz, 2H, H<sub>c</sub>), 7.20 (d,  $J = 8.6$  Hz, 2H, H<sub>d</sub>), 6.72 (d,  $J = 8.9$  Hz, 2H, H<sub>b</sub>), 3.10 (pt,  $J = 8.6$  Hz, 16H, H<sub>i</sub>), 2.98 (s, 6H, H<sub>a</sub>), 1.61 (quin,  $J = 8.0$  Hz, 16H, H<sub>h</sub>), 1.36 (sex,  $J = 7.4$  Hz, 16H, H<sub>g</sub>), 0.97 (t,  $J = 7.4$  Hz, 24 H, H<sub>f</sub>).  $\delta_{\text{C}}$  (125 MHz, CD<sub>3</sub>CN) 151.8, 133.8, 132.1, 127.2, 124.7, 112.9, 109.8, 95.3, 87.8, 59.4, 40.4, 24.4, 20.4, 13.9. Anal. Calcd (found) % for C<sub>48</sub>H<sub>86</sub>N<sub>4</sub>O<sub>18</sub>Mo<sub>6</sub>: C, 36.42 (36.54); H, 5.47 (5.40); N, 3.53 (3.57).  $m/z = 549$  [C<sub>16</sub>H<sub>14</sub>N<sub>2</sub>Mo<sub>6</sub>O<sub>18</sub>]<sup>2-</sup>, 1098 [H[C<sub>16</sub>H<sub>14</sub>N<sub>2</sub>Mo<sub>6</sub>O<sub>18</sub>]]<sup>1-</sup>, [(NBu<sub>4</sub>)[C<sub>16</sub>H<sub>14</sub>N<sub>2</sub>Mo<sub>6</sub>O<sub>18</sub>]]<sup>1-</sup>. FTIR: 2960 (m); 2872 (m); 2198 (m); 1606 (m); 1581 (m); 1522 (m); 1480 (m); 1362 (m); 1200 (w); 1196 (vw); 1167 (vw); 1132 (w); 1063 (vw); 1029 (vw); 974 (m); 944 (vs); 769 (vs). UV-vis (MeCN)  $\lambda$ , nm ( $\epsilon$ , M<sup>-1</sup> cm<sup>-1</sup>): 247.5 (36.2 × 10<sup>3</sup>); 292.0 (44.5 × 10<sup>3</sup>); 421.0 (41.2 × 10<sup>3</sup>).

**Synthesis of [(C<sub>4</sub>H<sub>9</sub>)<sub>4</sub>N]<sub>3</sub>[PW<sub>11</sub>O<sub>39</sub>{O(Si-PhNH<sub>2</sub>)<sub>2</sub>}] (11).** (Bu<sub>4</sub>N)<sub>4</sub>[H<sub>3</sub>PW<sub>11</sub>O<sub>39</sub>] (1.50 g, 0.411 mmol) was dissolved in acetonitrile:water mixture (52.5:22.5 mL) at 0 °C in an ice bath. A solution of *p*-aminophenyl trimethoxysilane (0.20 g, 0.937 mmol) in acetonitrile (15 mL) was added dropwise to the former solution, with vigorous stirring. The pH of the solution was set and held at 2.3 for 15 minutes by the drop-wise addition of 1 M HCl, and which was then left to stir overnight at room temperature, affording a light-red solution and precipitate. This was filtered and dissolved in MeCN before being filtered to remove unreacted (Bu<sub>4</sub>N)<sub>4</sub>[H<sub>3</sub>PW<sub>11</sub>O<sub>39</sub>] solid. A solution of tetrabutylammonium bromide (0.85 g, 2.646 mmol) was added and the solution then layered with ethanol and stirred at room temperature for 30 minutes resulting in the formation of a dark brown precipitate. The precipitate was then collected on a fine frit and washed with ethanol (3 × 10 mL), then dissolved in the minimum of acetonitrile, followed by the addition of triethylamine (52.5  $\mu$ L) with stirring to fully deprotonate the amines. An excess of tetrabutylammonium bromide (*c.a.* 2.0 g) was added, and the solution layered with ethanol resulting in a brown precipitate. This was filtered, washed with ethanol (3 × 10 mL) and ether (3 × 10 mL) to give the product as a brown solid (1 g, 0.274 mmol, 66%).  $\delta_{\text{H}}$  (300 MHz, CD<sub>3</sub>CN) 7.52 (d,  $J = 8.5$  Hz, 4H, H<sub>c</sub>), 6.72 (d,  $J = 8.5$  Hz, 4H, H<sub>b</sub>), 4.41 (s, 4H, H<sub>a</sub>), 3.09 (pt,  $J = 8.5$  Hz, 24H, H<sub>g</sub>), 1.61 (quin,  $J = 7.9$  Hz, 24H, H<sub>f</sub>), 1.37 (sex,  $J = 7.4$  Hz, 24H, H<sub>e</sub>), 0.98 (t,  $J = 7.3$  Hz, 36 H, H<sub>d</sub>).  $\delta_{\text{P}}$  (202 MHz, CD<sub>3</sub>CN) -13.49 (s, 1P). Anal. Calcd (found) %

for  $\text{PW}_{11}\text{O}_{40}\text{Si}_2\text{C}_{60}\text{H}_{120}\text{N}_5$ : C, 19.68 (19.72); H, 3.25 (3.31); N, 1.91 (1.94).  $m/z = 1588.28$   $[(\text{Bu}_4\text{N})[\text{C}_{12}\text{H}_{12}\text{N}_2\text{PW}_{11}\text{O}_{40}\text{Si}_2]]^2$ . FTIR: 2960 (m); 2935 (m); 2874 (m); 1620 (m); 1600 (m); 1508 (w); 1480 (m); 1460 (m); 1379 (w); 1274 (vw); 1188 (m); 1130 (s); 1108 (m); 1064 (s); 1033 (w); 958 (vs); 900 (w); 864 (vs); 814 (vs); 706 (w); 656 (m). UV-vis (MeCN)  $\lambda$ , nm ( $\epsilon$ ,  $\text{M}^{-1} \text{cm}^{-1}$ ): 262.5 ( $64.0 \times 10^3$ ).

## X-ray Crystallographic Details

**Sample Growth, Data Collection and Refinement.** Crystals of **1**·MeCN, **2**, **5**, **6**·MeCN, **7**·0.25Et<sub>2</sub>O and **10**·0.25Et<sub>2</sub>O·0.5MeCN (CCDC deposition numbers 1553805 to 1553810) were obtained by room temperature diffusion of diethyl ether vapor into acetonitrile. Structures of **4**, **8** and **9** were previously published.<sup>4</sup> Data were collected on Oxford Diffraction XCalibur 3 diffractometer, or a Rigaku AFC 12 goniometer equipped with an enhanced sensitivity (HG) Saturn724+ detector and FR-E+ SuperBright molybdenum rotating anode generator with HF Varimax optics (100  $\mu\text{m}$  focus). Data reduction, cell refinement and absorption correction was carried out using Agilent Technologies CrysAlisPro<sup>8</sup> or Rigaku CrystalClear-SM Expert software,<sup>9</sup> and solved using SHELXS-2014<sup>10</sup> or SIR-92<sup>11</sup> *via* WinGX.<sup>12</sup> Refinement was achieved by full-matrix least-squares on all  $F_0^2$  data using SHELXL-2014<sup>13</sup> and molecular graphics were prepared using ORTEP-3<sup>14</sup> or Mercury 3.8.<sup>15</sup> Compound **1** required a twin refinement, compound **2** application of the SQUEEZE routine<sup>16</sup> to remove disordered solvent that would not refine adequately, and several structures required application of restraints (bond distances, thermal parameters) to disorder on cations, solvents and in **2** the hexamolybdate cluster. In **6**·MeCN and **10**·0.25Et<sub>2</sub>O·0.5MeCN disordered solvent was refined isotropically as isotropic refinement failed. Full crystallographic data and refinement details are presented in Table S1 and ORTEP representations of the asymmetric units of each structure in Figures S1 to S6.

**Significant Bond Lengths and Angles.** Variations in the bond lengths and angles of the organic conjugated systems of the anions, of relevance to electronic and optical properties, are discussed in the main paper. Table S2 summarizes bond lengths and angles of the  $\{\text{Mo}_6\text{O}_{18}\text{N}\}$  units, that are very consistent with those of similar compounds in the literature.<sup>17</sup> In all structures, the Mo-N-C bond angle is closer to 180° than 120°, indicating significant Mo-N triple bond character. The compounds also show the typical imido-Lindqvist pattern of a shortened bond length from the imido-Mo ( $\text{Mo}^{\text{im}}$ ) to the central oxygen ( $\text{O}^{\text{c}}$ ), lengthened equatorial bond lengths from  $\text{Mo}^{\text{im}}$  to the oxygens bridging to the belt Mo positions ( $\text{Mo}^{\text{b}}$ ), and a lengthened axial bond length from the *trans*-Mo ( $\text{Mo}^{\text{t}}$ ) to  $\text{O}^{\text{c}}$ . There is, however, no consistent pattern in the terminal Mo=O distances which are typically in the range of 1.65 to 1.70 Å. Differences in specific bond lengths between the structures are generally too small to be statistically significant but there are significant variations in the Mo-N-C bond angle (from 162.55 to 176.0°). However, as these follow no clear pattern with the known properties of the attached aryl groups (e.g. electron donor/electron acceptor) they are more likely driven by crystal packing, than electronic factors.

**Table S1.** Crystallographic Data and Refinement Details for **1**·MeCN, **2**, **5**, **6**·MeCN, **7**·0.25Et<sub>2</sub>O and **10**·0.25Et<sub>2</sub>O·0.5MeCN

	<b>1</b> ·MeCN	<b>2</b>	<b>5</b>	<b>6</b> ·MeCN	<b>7</b> ·0.25Et <sub>2</sub> O	<b>10</b> ·0.25Et <sub>2</sub> O·0.5MeCN
Formula	C <sub>40</sub> H <sub>79</sub> IMo <sub>6</sub> N <sub>4</sub> O <sub>18</sub>	C <sub>40</sub> H <sub>77</sub> Mo <sub>6</sub> N <sub>3</sub> O <sub>18</sub>	C <sub>40</sub> H <sub>82</sub> Mo <sub>6</sub> N <sub>4</sub> O <sub>18</sub>	C <sub>48</sub> H <sub>83</sub> IMo <sub>6</sub> N <sub>4</sub> O <sub>18</sub>	C <sub>47</sub> H <sub>82.50</sub> Mo <sub>6</sub> N <sub>4</sub> O <sub>20.25</sub>	C <sub>50.5</sub> H <sub>91.75</sub> Mo <sub>6</sub> N <sub>4.25</sub> O <sub>18.5</sub>
<i>M</i>	1606.61	1463.69	1482.73	1706.72	1603.31	1630.17
cryst syst	Triclinic	Triclinic	Monoclinic	Monoclinic	Monoclinic	Monoclinic
space group	<i>P</i> -1	<i>P</i> -1	<i>P</i> 2 <sub>1</sub> /n	<i>P</i> 2 <sub>1</sub> /n	<i>P</i> 2 <sub>1</sub> /n	<i>P</i> 2 <sub>1</sub> /c
<i>a</i> /Å	12.1154(3)	12.3617(2)	17.356(1)	11.4858(3)	11.4858(3)	12.4494(2)
<i>b</i> /Å	12.1829(4)	19.1579(3)	15.645(1)	38.134(1)	38.134(1)	23.7848(4)
<i>c</i> /Å	19.6204(6)	25.2441(4)	20.484(1)	14.2817(5)	14.2817(5)	21.9894(4)
<i>α</i> /deg	93.785(2)	107.135(2)	90	90	90	90
<i>β</i> /deg	97.680(2)	94.445(1)	104.252(1)	91.649(2)	91.649(2)	103.573(2)
<i>γ</i> /deg	93.375(2)	100.815(1)	90	90	90	90
<i>U</i> /Å <sup>3</sup>	2857.0(2)	5555.1(2)	5390.9(6)	6252.8(3)	6252.8(3)	6329.4(2)
<i>Z</i>	2	4	4	4	4	4
<i>T</i> /K	140(2)	140(2)	100(2)	140(2)	100(2)	100(2)
<i>μ</i> /mm <sup>-1</sup>	1.883	1.379	1.423	1.727	1.236	1.221
Cryst. size/mm	0.17 × 0.08 × 0.04	0.3 × 0.25 × 0.15	0.19 × 0.04 × 0.04	0.33 × 0.18 × 0.03	0.15 × 0.09 × 0.04	0.34 × 0.05 × 0.02
Cryst. description	Orange plate	Orange block	Dark red prism	Orange plate	Red-orange block	Red needle
<i>λ</i> /Å	0.71073	0.71073	0.71073	0.71073	0.71073	0.71073
No. reflns collected	23119	112337	69741	37148	86181	89587
No. of indep. reflns ( <i>R</i> <sub>int</sub> )	23129 [R(int) = 0.00]	36262 [R(int) = 0.0577]	12362 [R(int) = 0.0742]	14331 [R(int) = 0.0423]	14275 [R(int) = 0.0724]	14538 [R(int) = 0.0506]
<i>θ</i> <sub>max</sub> /deg (completeness)	25.00 (99.8%)	25.00 (99.1%)	25.20 (99.8%)	25.24 (99.8%)	25.24 (99.9%)	25.24 (99.95)
Reflections with <i>I</i> > 2σ( <i>I</i> )	17488	19963	12046	10815	12713	12090
Goodness-of-fit on <i>F</i> <sup>2</sup>	0.994	1.019	1.220	1.059	1.204	0.990
final <i>R</i> <sub>1</sub> , <i>wR</i> <sub>2</sub> [ <i>I</i> > 2σ( <i>I</i> )] <sup>a</sup>	<i>R</i> <sub>1</sub> = 0.0403, <i>wR</i> <sub>2</sub> = 0.0966	<i>R</i> <sub>1</sub> = 0.0585, <i>wR</i> <sub>2</sub> = 0.1283	<i>R</i> <sub>1</sub> = 0.039, <i>wR</i> <sub>2</sub> = 0.100	<i>R</i> <sub>1</sub> = 0.0480, <i>wR</i> <sub>2</sub> = 0.0859	<i>R</i> <sub>1</sub> = 0.0707, <i>wR</i> <sub>2</sub> = 0.1380	<i>R</i> <sub>1</sub> = 0.0384, <i>wR</i> <sub>2</sub> = 0.0972
(all data)	<i>R</i> <sub>1</sub> = 0.0626, <i>wR</i> <sub>2</sub> = 0.1025	<i>R</i> <sub>1</sub> = 0.1201, <i>wR</i> <sub>2</sub> = 0.1445	<i>R</i> <sub>1</sub> = 0.040, <i>wR</i> <sub>2</sub> = 0.100	<i>R</i> <sub>1</sub> = 0.0732, <i>wR</i> <sub>2</sub> = 0.0914	<i>R</i> <sub>1</sub> = 0.0779, <i>wR</i> <sub>2</sub> = 0.1405	<i>R</i> <sub>1</sub> = 0.0512, <i>wR</i> <sub>2</sub> = 0.1032
Peak and hole/e Å <sup>-3</sup>	1.521 and -1.530	1.917 and -1.102	1.24 and -1.30	1.606 and -1.387	1.361 and -1.655	1.440 and -0.807

**Table S2** Significant bond lengths (Å) and angles (°) of the {Mo<sub>6</sub>O<sub>18</sub>N} clusters of **1**, **2** and **4** to **10**.<sup>a</sup>

	C-N-Mo <sup>im</sup>	N-Mo <sup>im</sup>	Mo <sup>im</sup> -O <sup>c</sup>	Mo <sup>t</sup> -O <sup>c</sup>	Mo <sup>im</sup> -O <sup>b</sup> (average)	Mo <sup>t</sup> -O <sup>b</sup> (average)
<b>1</b>	164.8 (3)	1.743 (4)	2.199 (3)	2.375 (3)	1.949 (3)	1.922 (3)
<b>2</b>	170.80 (4)	1.737 (4)	2.219 (3)	2.336 (3)	1.948 (3)	1.918 (3)
<b>4</b>	173.3 (3)	1.738 (3)	2.206 (2)	2.361 (2)	1.952 (3)	1.920 (3)
<b>5</b>	162.55 (3)	1.738 (3)	2.210 (2)	2.350 (2)	1.955 (3)	1.945 (3)
<b>6</b>	165.3(4)	1.738 (4)	2.187(3)	2.350(3)	1.954 (4)	1.919 (3)
<b>7</b>	163.46 (6)	1.748 (6)	2.190 (5)	2.350 (5)	1.966 (5)	1.934 (5)
<b>8</b>	172.7 (11)	1.734 (11)	2.234 (8)	2.341 (8)	1.946 (8)	1.941 (9)
<b>9</b>	176.0 (7)	1.738 (8)	2.196 (5)	2.352 (5)	1.947 (6)	1.917 (7)
<b>10</b>	168.32 (3)	1.737 (3)	2.219 (2)	2.355 (2)	1.946 (2)	1.920 (3)

<sup>a</sup> In cases of disorder on the hexamolybdate anion (**2**) or multiple anions in the asymmetric unit (**2** and **9**) the tabulated distances and angles in the first four columns are averages. Mo<sup>im</sup> is the imido carrying Mo atom, Mo<sup>t</sup> the Mo *trans* to the imido (across the central oxygen), O<sup>c</sup> the central oxygen, O<sup>b</sup> the oxygens bridging to belt Mo positions to which distances are necessarily averaged. Terminal Mo=O distances in all structures are in the range of 1.65 to 1.70 Å and show no consistent pattern. The structures of **4**, **8** and **9** were previously published.<sup>4</sup>

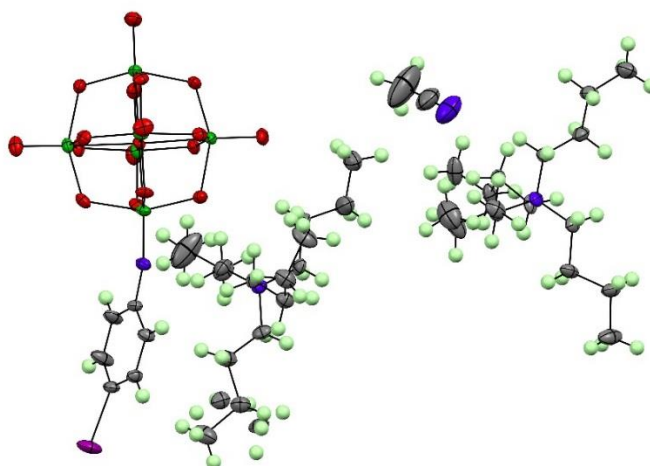


**Figure S1** ORTEP representation of the asymmetric unit in **1**·MeCN. Thermal ellipsoids are at the 30% probability level. Color scheme: Mo is green; O, red; C, gray; N, blue; H atoms are represented by green spheres of arbitrary radii.

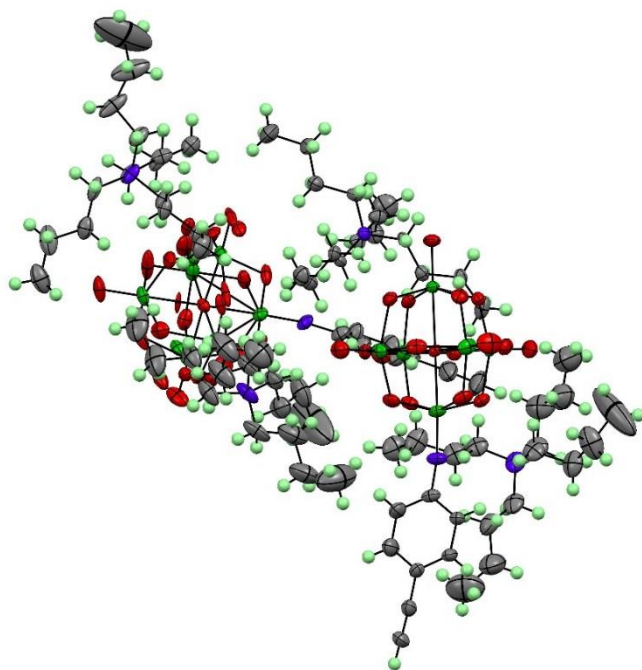


**Figure S2** ORTEP representation of the asymmetric unit in **2**. Thermal ellipsoids are at the 30% probability level. Color scheme as Figure S1.

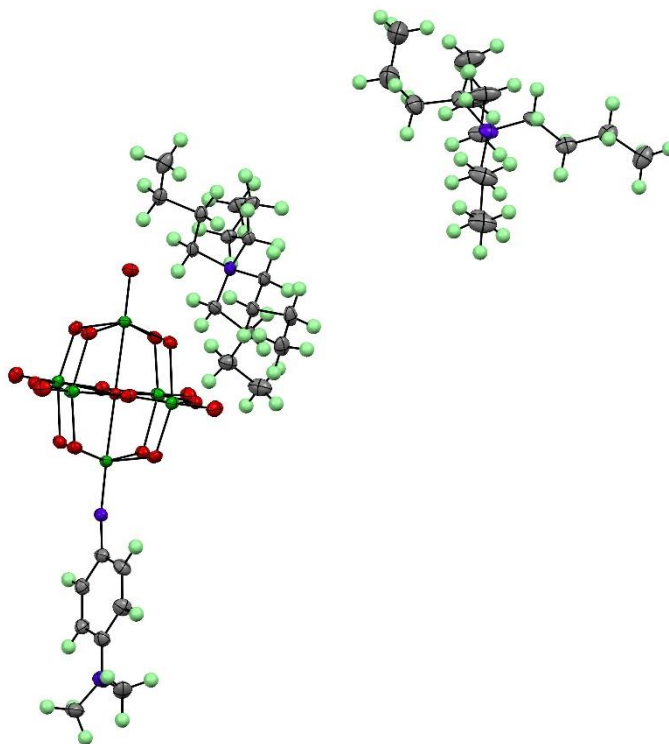


**Figure S3** ORTEP representation of the asymmetric unit in **5**. Thermal ellipsoids are at the 30% probability level. Color scheme: as Figure S1, atom labels omitted for clarity.

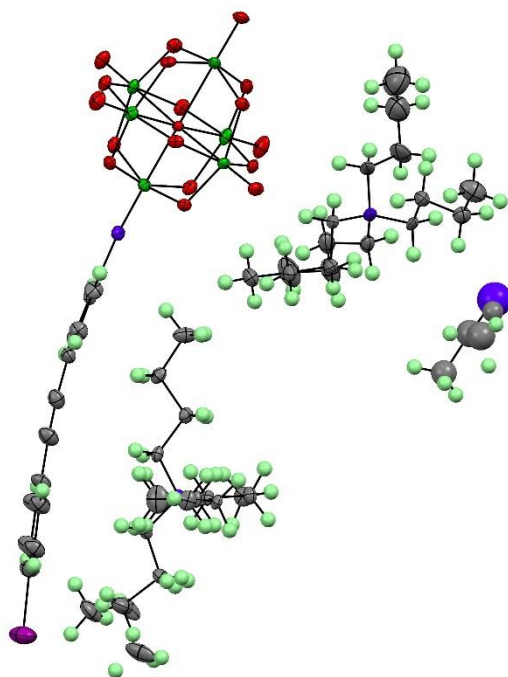


**Figure S4** ORTEP representation of the asymmetric unit in **6**·MeCN. Thermal ellipsoids are at the 30% probability level. Color scheme: as Figure S1, atom labels omitted for clarity.

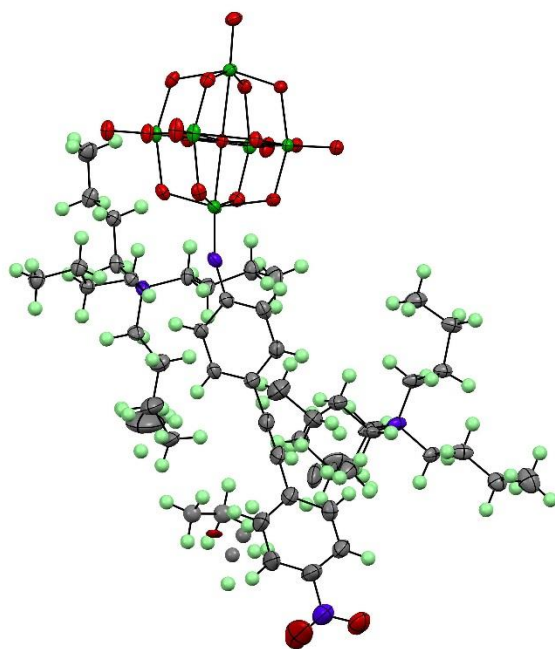


**Figure S5** ORTEP representation of the asymmetric unit in **6**·MeCN. Thermal ellipsoids are at the 30% probability level. Color scheme: as Figure S1, atom labels omitted for clarity.

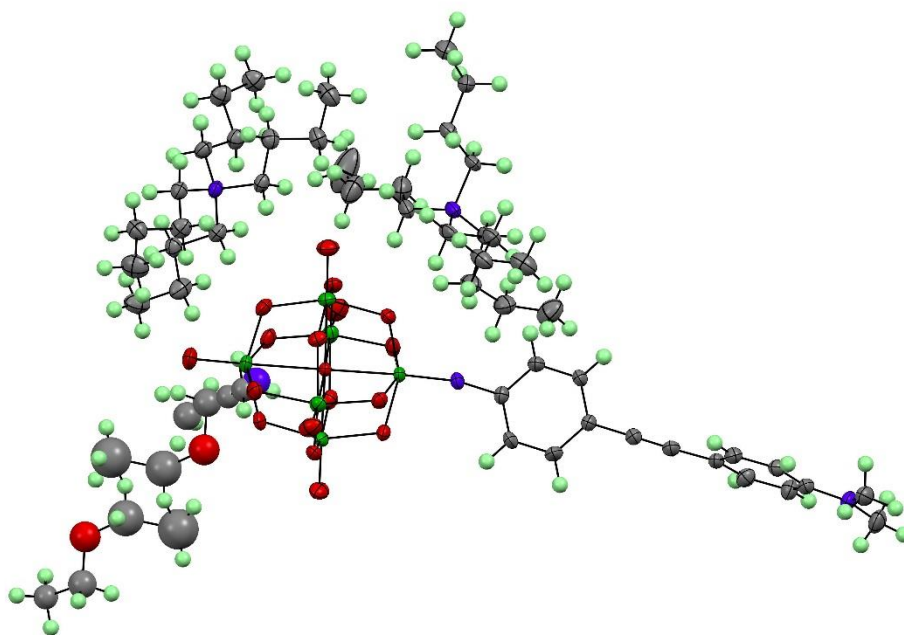


**Figure S6** ORTEP representation of the asymmetric unit in **10**·0.25Et<sub>2</sub>O·0.5MeCN. Thermal ellipsoids are at the 30% probability level. Color scheme: as Figure S1, atom labels omitted for clarity.

### **Additional Raman Spectra**

Raman spectra of compounds **5**, **6**, **3**, **7**, **12** and **13** are displayed below in Figures S7 to S9.

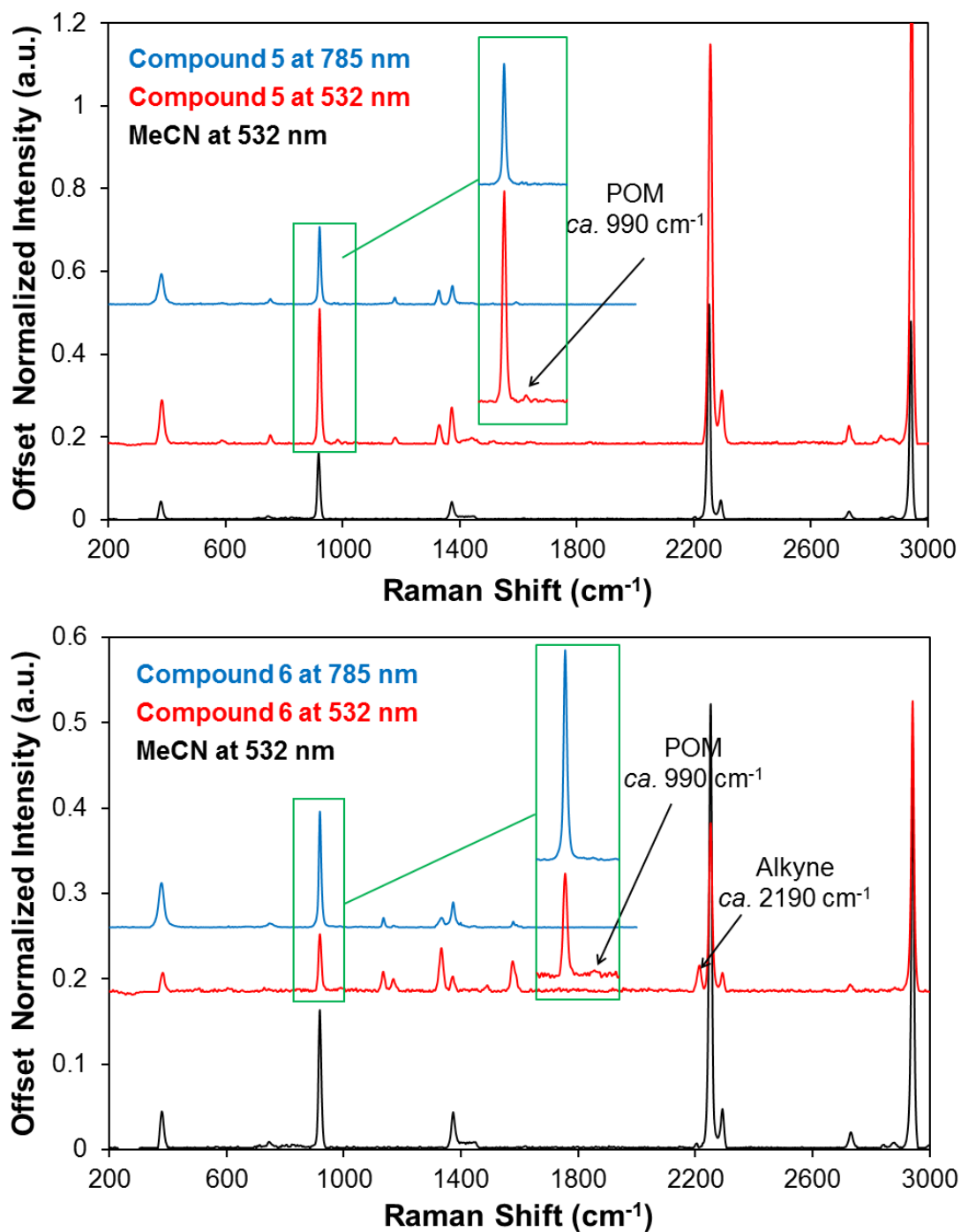


**Figure S7** Raman spectra of  $[\text{NBu}_4]_2[\text{Mo}_6\text{O}_{18}\text{NPhNMe}_2]$  (**5**) and  $[\text{NBu}_4]_2[\text{Mo}_6\text{O}_{18}\text{NPhCCPhI}]$  (**6**) showing significantly weaker enhancement of the POM/imido  $990\text{ cm}^{-1}$  bands at  $532\text{ nm}$  compared to **1**, **3** or **10** (consider intensity of nearby MeCN signal vs intensity of POM band).

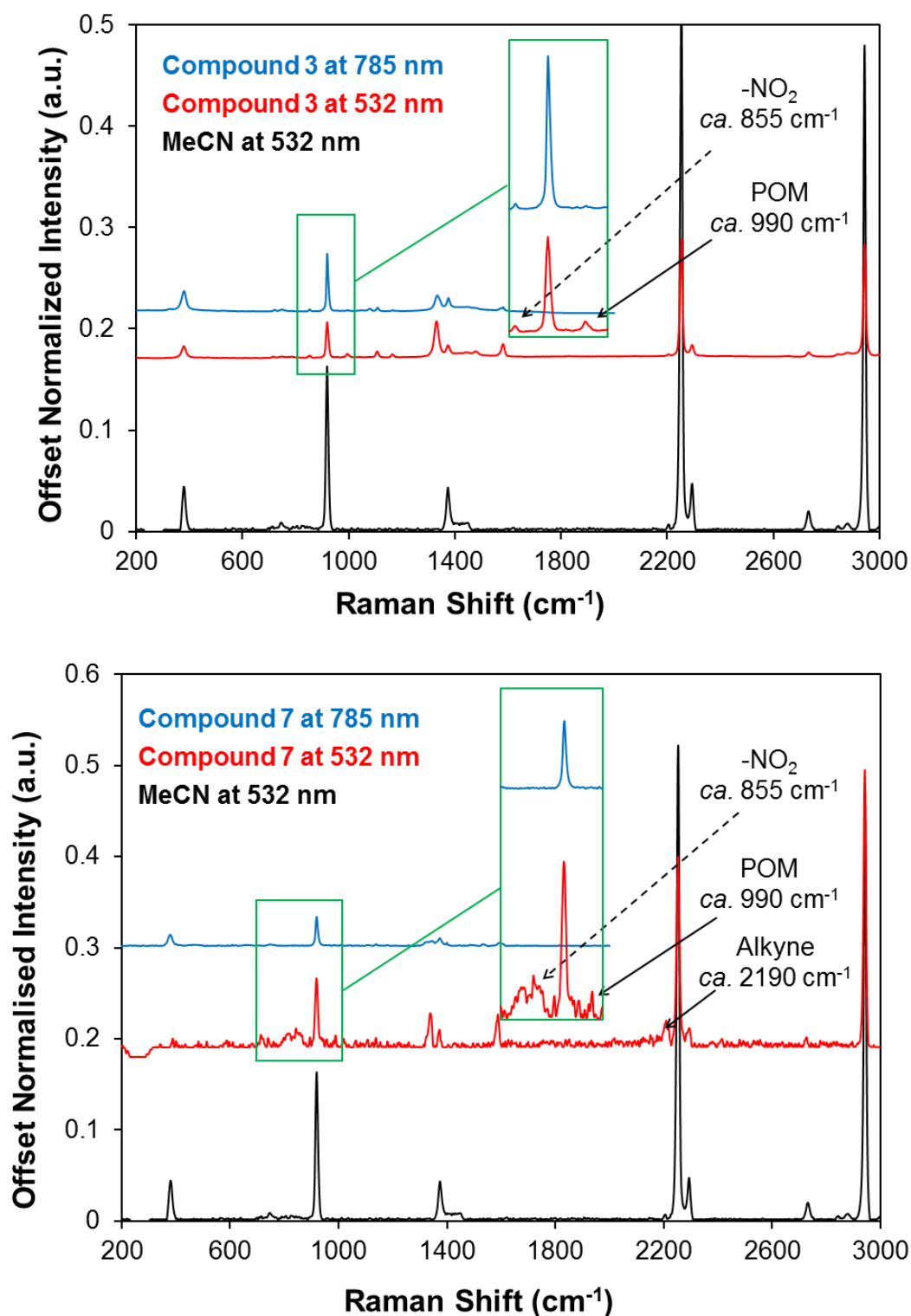


**Figure S8** Raman spectra of  $[\text{NBu}_4]_2[\text{Mo}_6\text{O}_{18}\text{NPhNO}_2]$  (**3**) and  $[\text{NBu}_4]_2[\text{Mo}_6\text{O}_{18}\text{NPhCCPhNO}_2]$  (**7**) showing weakened enhancement of the POM/imido 990 cm<sup>-1</sup> bands at 532 nm in the extended compound, despite greater absorption at the excitation wavelength. Enhancement of the 855 cm<sup>-1</sup> - NO<sub>2</sub> band is also suppressed by comparison with POM-free nitro compounds **12** and **13** (Fig. S9). Raman bands at ca. 1335 cm<sup>-1</sup> and 1585 cm<sup>-1</sup> in both samples may also be associated with -NO<sub>2</sub> but cannot unambiguously be assigned due to similar bands in several nitro-free samples.

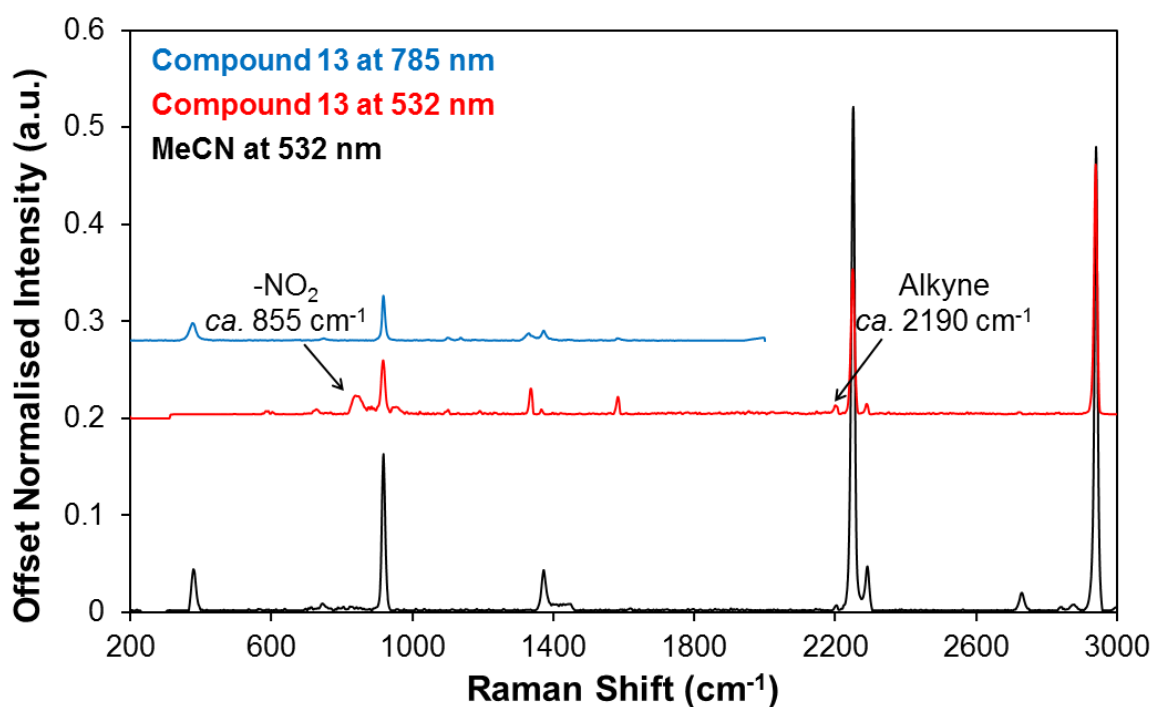
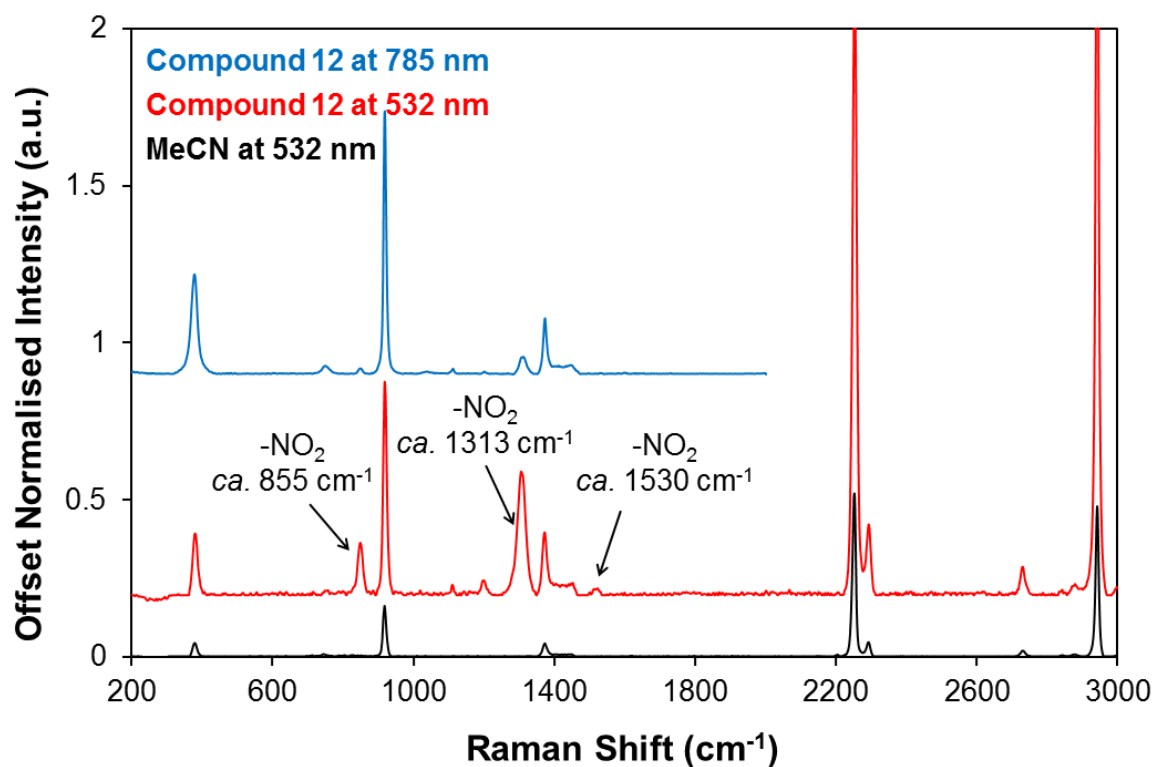


**Figure S9** Raman spectra of *p*-Me<sub>2</sub>NPhNO<sub>2</sub> (**12**) and *p*-Me<sub>2</sub>NPhCCPhNO<sub>2</sub> (**13**) showing strong enhancement of the 855 cm<sup>-1</sup> -NO<sub>2</sub> band with 532 nm excitation, even in **12** which appears effectively transparent at this wavelength. Raman bands at ca. 1335 cm<sup>-1</sup> and 1585 cm<sup>-1</sup> in **13** may also be associated with -NO<sub>2</sub> but cannot unambiguously be assigned due to similar bands in several nitro-free samples. The small band slightly below 1000 cm<sup>-1</sup> is of uncertain origin but has a significantly different frequency (960 cm<sup>-1</sup>) to the 990 cm<sup>-1</sup> associated with the POM/imido.

## UV-vis Spectra of Nitro Analogues **12** and **13**

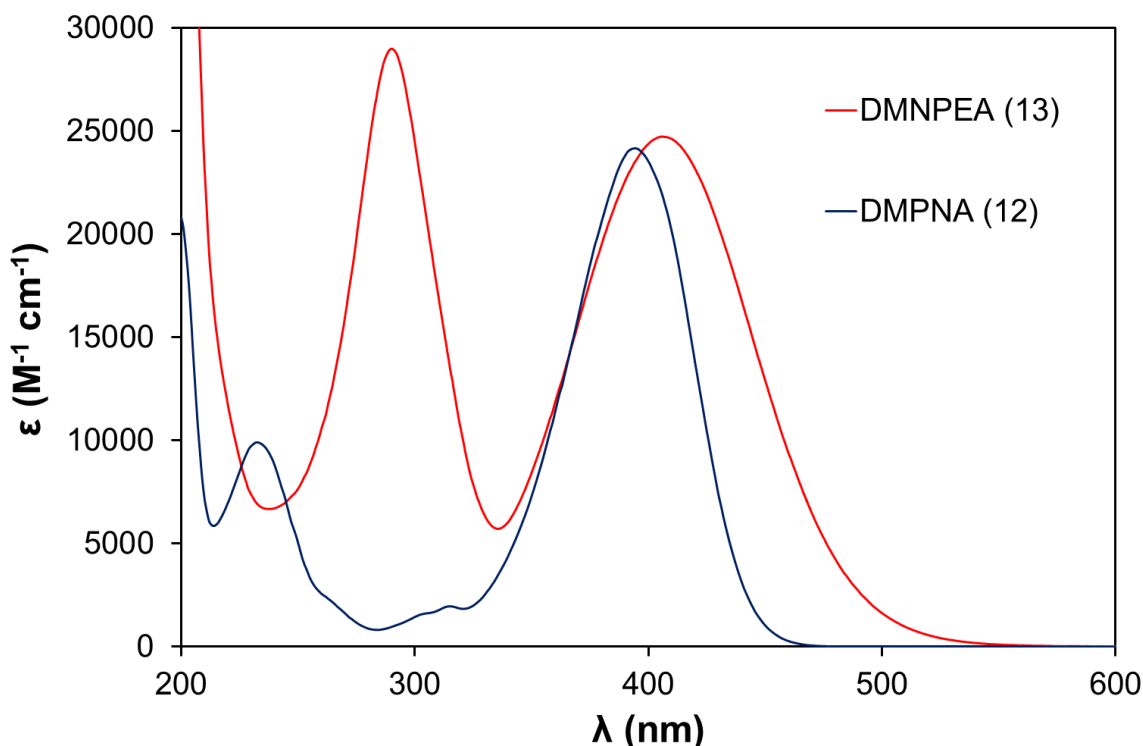


**Figure S10.** Electronic absorption spectra of organic nitro compounds **12** and **13** in MeCN at 298 K.

**Table S3** UV-vis data for organic nitro compounds **12** and **13** in MeCN at 298 K.

	$\lambda_{\max}$ / nm <sup>a</sup> ( $\epsilon$ , 10 <sup>3</sup> M <sup>-1</sup> cm <sup>-1</sup> )	$E_{\max}$ (eV)	assignment
<b>12</b>	233 (9.9)	5.32	$\pi \rightarrow \pi^*$
	394 (24.2)	3.15	N <sub>Aryl</sub> →NO <sub>2</sub> CT
<b>13</b>	290 (28.7)	4.28	$\pi \rightarrow \pi^*$
	406 (25.0)	3.05	N <sub>Aryl</sub> →NO <sub>2</sub> CT

## Example Stark Spectra and Fits

The six examples below in Figures S11 and S12 show typical low temperature (77 K) absorption spectra as butyronitrile glasses, contributing Gaussian curves to the fits, Stark spectra, fits, and overall contributions of the 0<sup>th</sup>, 1<sup>st</sup> and 2<sup>nd</sup> derivatives for **1**, **3**, **5**, **6**, **8** and **10**. This provides examples of systems with no significant resonance donor or acceptor (-I), strong acceptor (-NO<sub>2</sub>), weak-to-moderate resonance donor (pyrrole) and strong donor (-NMe<sub>2</sub>) in the 4-position of the phenyl or diphenylacetylene bridge, and shows that in the absence of resonance donors the spectra are dominated by first derivative (polarizability) contributions, with minimal participation from the second derivative (charge transfer). Note that in the case of **1**, 0<sup>th</sup> derivative contributions have been excluded from the fit. Including them brings minor improvements to the fit but allows inclusion of a 2<sup>nd</sup> derivative contribution that may not be real. For **3**, excluding 0<sup>th</sup> derivative contributions slightly worsens the fit, but produces only relatively minor differences in calculated transition dipole moment changes that result from the 2<sup>nd</sup> derivative. These would not affect the overall conclusion of the study.

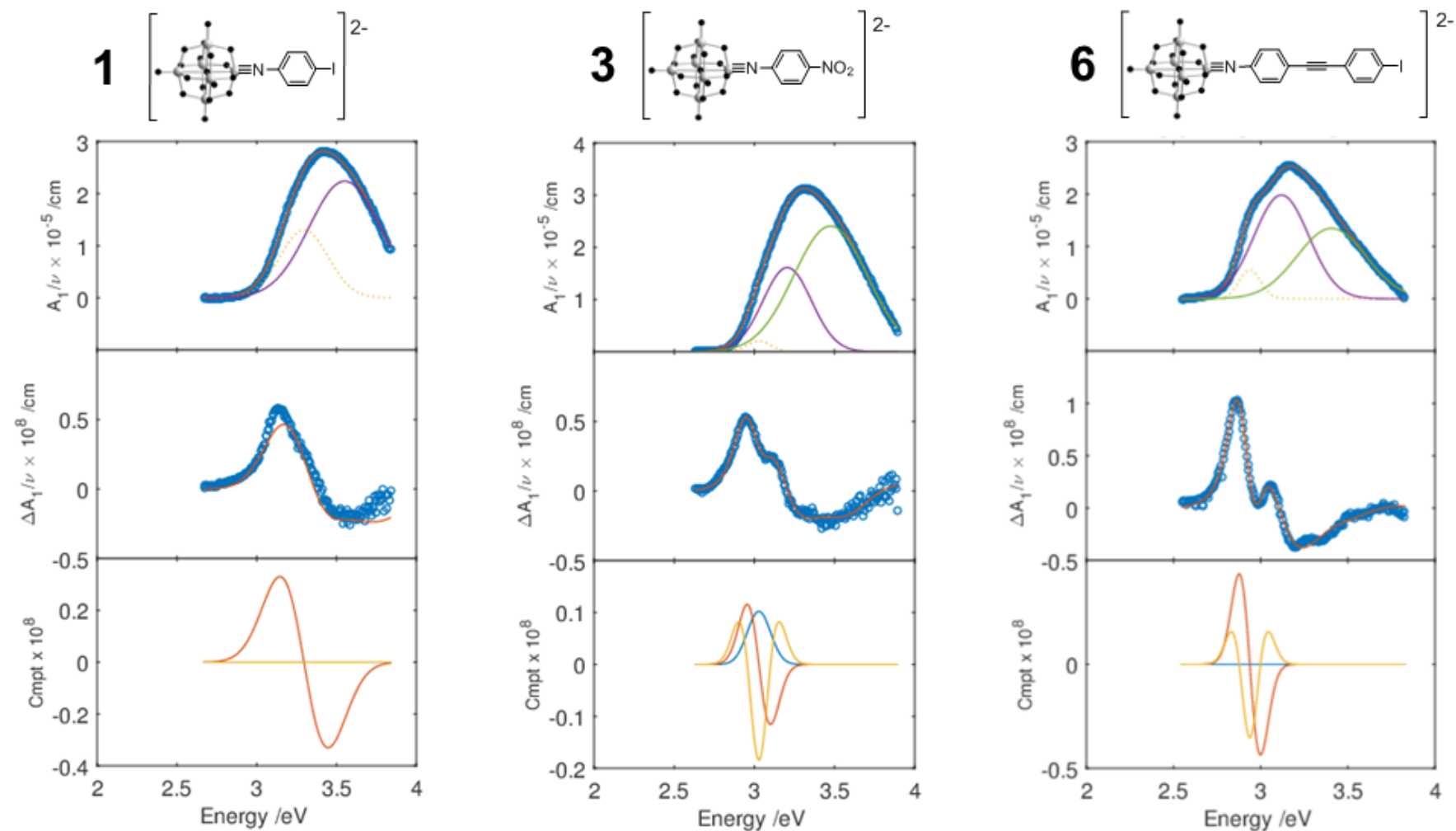


**Figure S11** Stark spectra and fits for **1**, **3** and **6** at 77 K. For each example: **Top** – absorption spectrum (blue circles), fit (red line) and contributing Gaussian curves (purple, yellow, green); **Middle** – Stark spectrum (blue circles), fit (orange line); **Bottom** – Overall contribution of derivatives, 0<sup>th</sup> (blue), 1<sup>st</sup> (orange) and 2<sup>nd</sup> (yellow). In these compounds with no resonance donor, the 1<sup>st</sup> derivative contribution (polarizability) is generally the most significant.

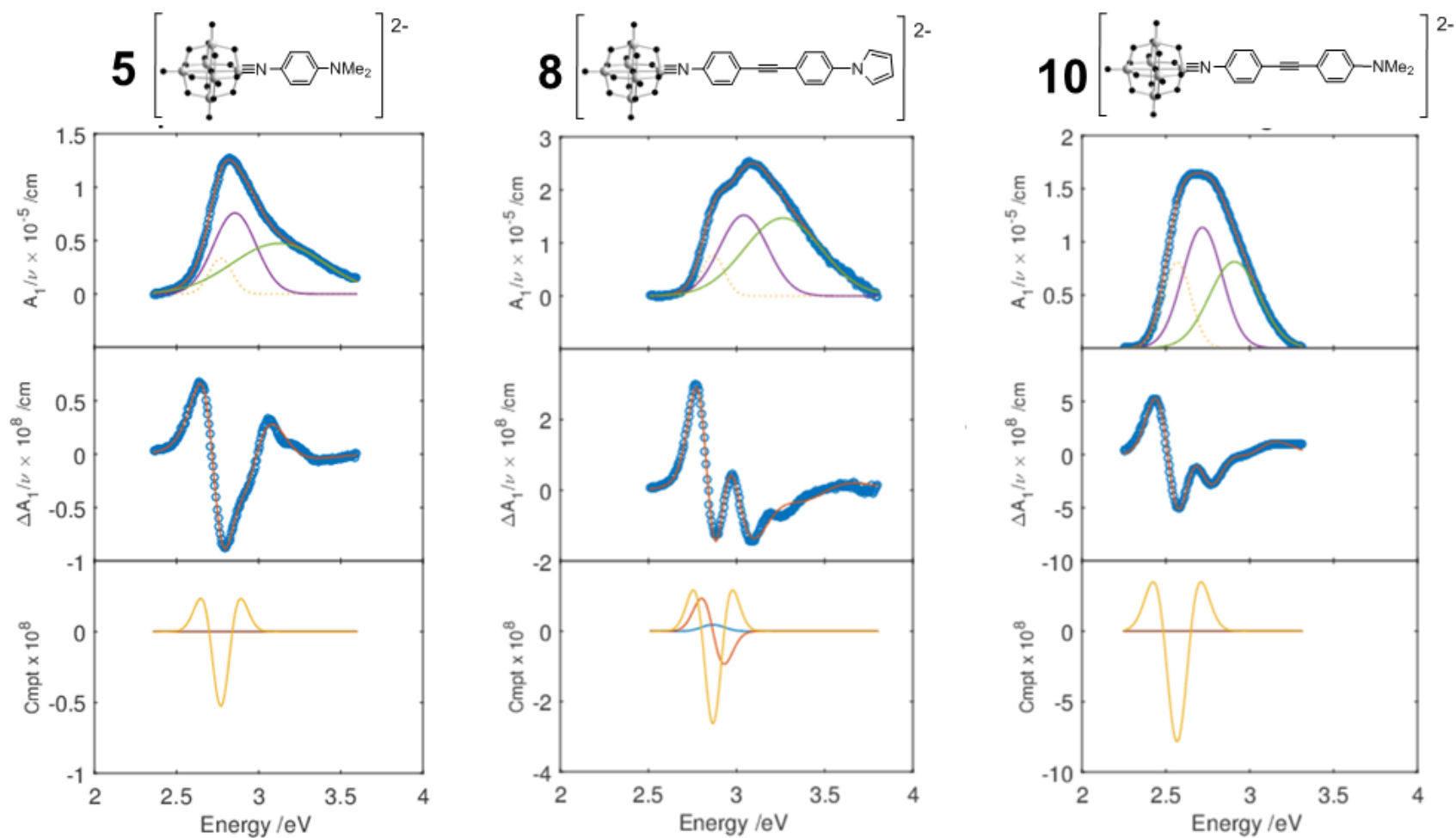


**Figure S12** Stark spectra and fits for **5**, **8** and **10** at 77 K. For each example: **Top** – absorption spectrum (blue circles), fit (red line) and contributing Gaussian curves (purple, yellow, green); **Middle** – Stark spectrum (blue circles), fit (orange line); **Bottom** – Overall contribution of derivatives,  $0^{\text{th}}$  (blue),  $1^{\text{st}}$  (orange) and  $2^{\text{nd}}$  (yellow). With the strong  $-\text{NMe}_2$  donor, the only significant contribution is the  $2^{\text{nd}}$  derivative contribution (charge transfer). With the weaker pyrrole donor  $2^{\text{nd}}$  derivative still dominates, but a significant contribution is made by the  $1^{\text{st}}$  derivative.

## DFT calculations

**Method.** DFT calculations were carried out using the ADF suite of programs.<sup>18</sup>

Geometry optimisation was carried out using the ADF triple- $\zeta$  TZP basis set with the zero-order regular approximation (ZORA) to account for relativistic effects.<sup>19</sup> A ‘small’ frozen core was employed for the molybdenum atoms. The generalized-gradient approximation (GGA) was employed in the geometry optimizations using the Beck and Perdew (BP86) exchange-correlation (XC) functional.<sup>20,21</sup> Calculations of the polarizability, second-order polarizability and electronic spectra used the RESPONSE and EXCITATION modules implemented in the ADF program<sup>22</sup> and were based on the optimized geometries. TD-DFT with the SAOP XC and ADF triple- $\zeta$  TZ2P basis set with no frozen core were used for these calculations.<sup>23</sup> Calculations in solvent (acetonitrile) were carried out using COSMO with Klamt atomic Radii.

**Results.** Previous calculations of NLO properties in imido-POMs<sup>24</sup> have used ADF but employed the older LB94 XC functional and smaller TZP basis set, and were gas phase only. The methods employed here should in principle be more accurate, although comparison of our results on **6** and **7** in the gas phase with the most directly comparable structures in the literature suggest they are likely to have yielded very similar results (Chart S1).

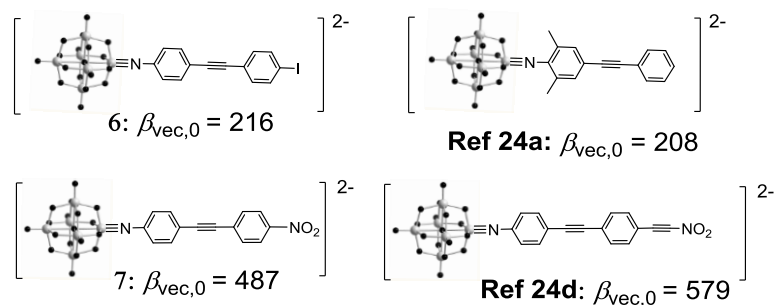


**Chart S1** Calculated, orientationally averaged static  $\beta$  values,  $\beta_{vec,0}$  ( $\times 10^{-30}$  esu) for compounds **6** and **7** versus closely related structures from the literature.

To our knowledge, calculations of this nature have not been previously carried out with a solvent correction. On large POM based systems, calculations of UV-vis transitions are very computationally expensive in solvent. Therefore, our calculated electronic spectra in solution are limited to **1**, **3**, **5** and **10** providing a subset that allows us to see the effect of with strong donor (-NMe<sub>2</sub>) and strong acceptor (-NO<sub>2</sub>) groups, those with neither strong donating nor accepting properties (-I), and the effect of extended conjugation (**10**). Calculations of  $\beta$  are less expensive and were carried out for all compounds in both phases, and electronic transitions were obtained for all compounds in the gas phase. Results of electronic spectra calculations for **1**, **3** and **5** are displayed in Fig. S13, in gas phase and with two different solvent corrections. The gas phase spectra of **1** and **5** are a reasonable match for our room temperature MeCN spectra of these compounds in terms of the position of the lowest energy band associated with the IHCT processes and NLO properties. In **3** however, the calculated band is red-shifted *ca.* 70 nm from its experimentally observed position. Solvent correction with both Klamt and Allinger atomic radii worsens the match between experiment and theory for all three compounds, with the lowest energy bands shifting up to 200 nm to the red. This effect is most pronounced in **5**, and least in **3**. Although the solvent correction worsens the match with experimental UV-vis data, it may still give a truer insight into the relative positions of the frontier orbitals (and thus NLO properties). As the solvent correction using Klamt radii gave a less dramatic red shift, and also was more successful in computation of  $\beta$  values, all subsequent solvent corrections use Klamt radii. The results of calculations for all compounds are summarized over the following pages.

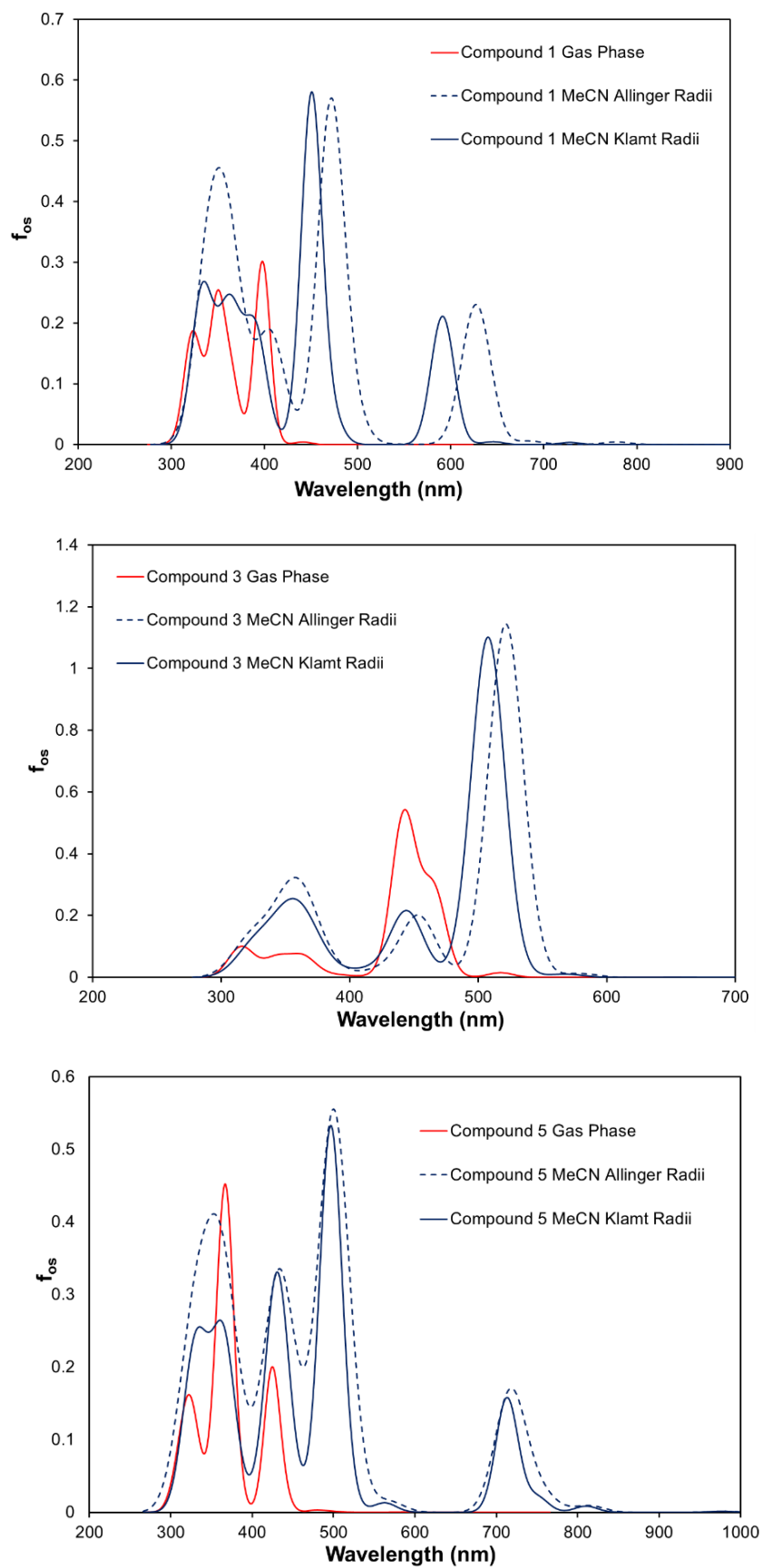
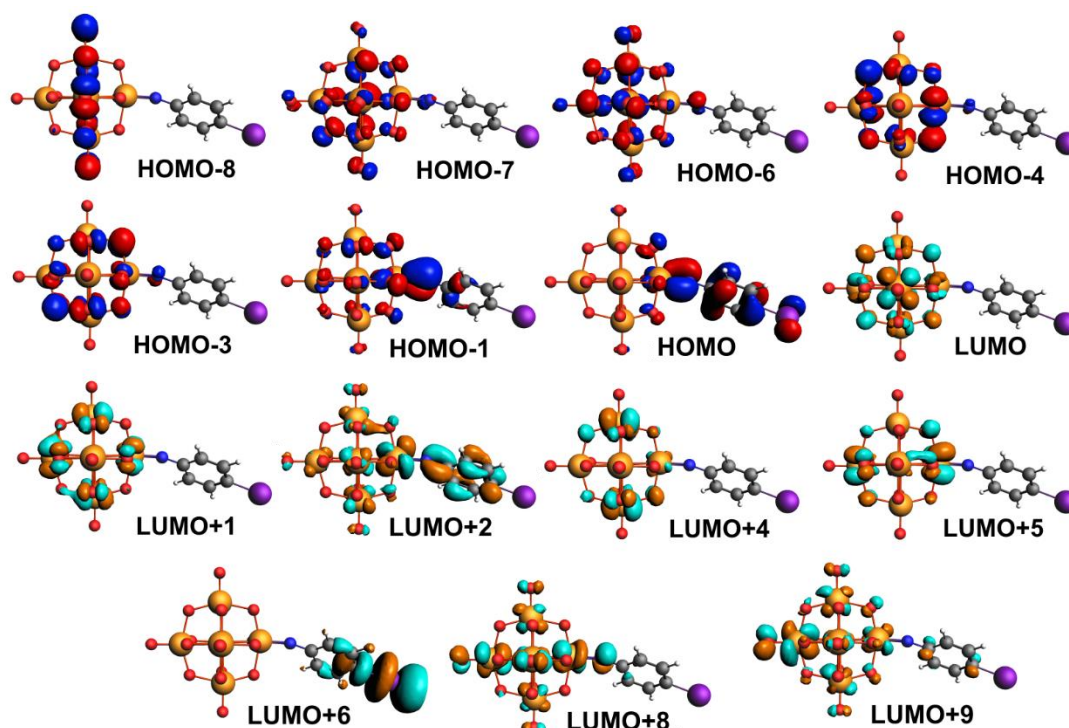


**Figure S13** Computed gas phase, and MeCN solution UV-vis spectra for **1**, **3** and **5**.

## TD-DFT Calculated Gas Phase Electronic Transitions of **1** to **10**

**Table S4** Calculated Gas Phase Electronic Transitions of Compound **1**

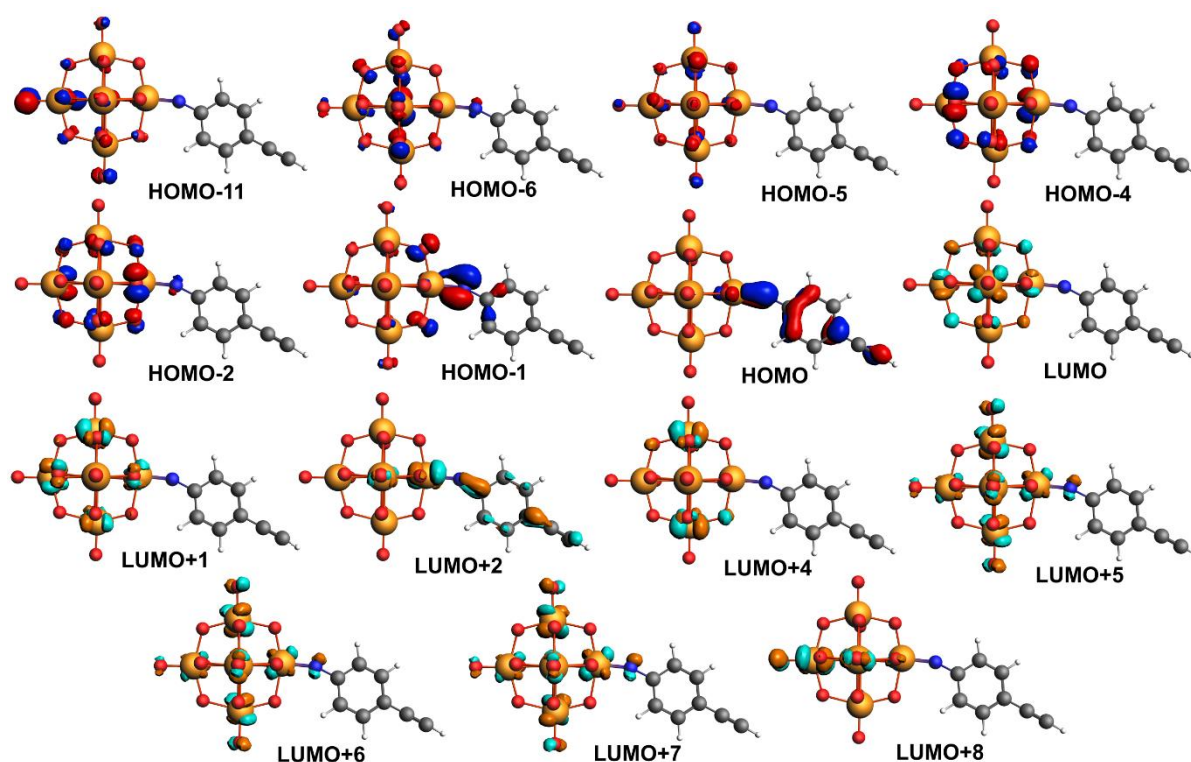
Transition Energy / eV	$f_{os}$	Orbital contributions
3.10	0.1664	HOMO $\rightarrow$ LUMO+8 (42%) HOMO $\rightarrow$ LUMO+2 (33%) HOMO $\rightarrow$ LUMO+9 (11%)
3.14	0.1461	HOMO $\rightarrow$ LUMO+8 (54%) HOMO $\rightarrow$ LUMO+2 (23%) HOMO $\rightarrow$ LUMO+9 (13%)
3.40	0.0328	HOMO-3 $\rightarrow$ LUMO (15%) HOMO-4 $\rightarrow$ LUMO+1 (14%) HOMO-3 $\rightarrow$ LUMO+2 (14%) HOMO-1 $\rightarrow$ LUMO+4 (11%) HOMO-4 $\rightarrow$ LUMO (10%)
3.55	0.1785	HOMO $\rightarrow$ LUMO+9 (48%) HOMO $\rightarrow$ LUMO+2 (10%) HOMO-1 $\rightarrow$ LUMO+6 (8%)
3.86	0.0405	HOMO-1 $\rightarrow$ LUMO+8 (14%) HOMO-3 $\rightarrow$ LUMO+8 (13%) HOMO-6 $\rightarrow$ LUMO+4 (13%) HOMO-4 $\rightarrow$ LUMO+8 (11%) HOMO-7 $\rightarrow$ LUMO+4 (11%)
3.88	0.0489	HOMO-6 $\rightarrow$ LUMO+4 (21%) HOMO-7 $\rightarrow$ LUMO+4 (15%) HOMO-6 $\rightarrow$ LUMO+5 (12%) HOMO-8 $\rightarrow$ LUMO+1 (11%) HOMO-3 $\rightarrow$ LUMO+8 (10%)



**Figure S14** Gas phase frontier orbitals involved in the significant UV-vis transitions of **1**. The strong, low energy HOMO  $\rightarrow$  LUMO+2 has little dipolar CT character as donor and acceptor orbitals are not very spatially separated. Other transitions show a mix of CT towards, and away from the POM to give overall weak dipole moment change.

**Table S5** Calculated Gas Phase Electronic Transitions of Compound **2**

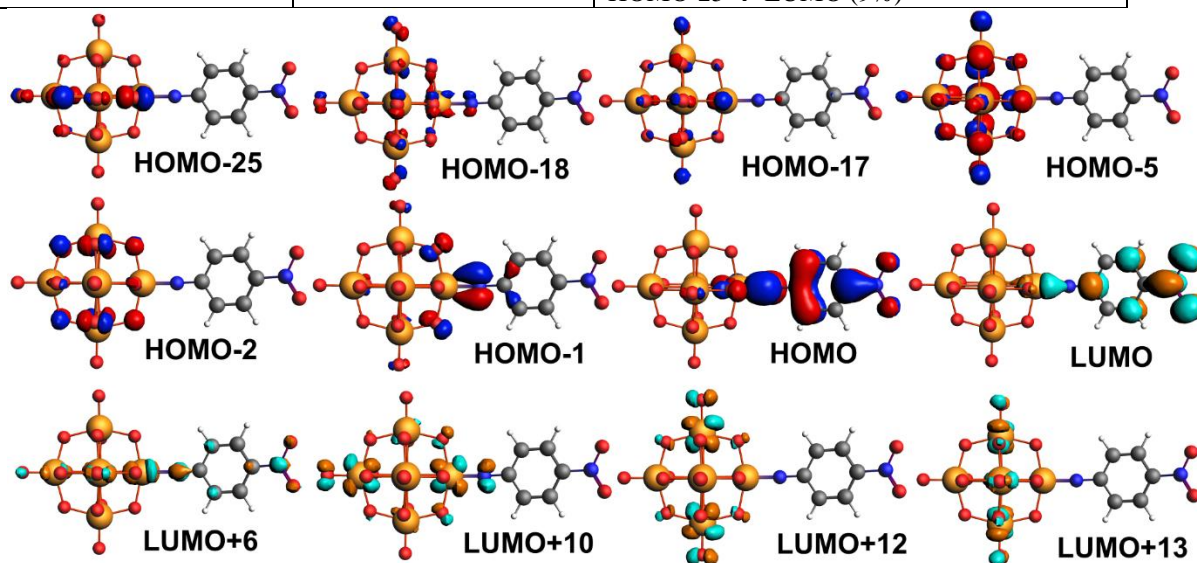
Transition Energy / eV	$f_{os}$	Orbital contributions
3.04	0.3927	HOMO $\rightarrow$ LUMO+2 (51%) HOMO $\rightarrow$ LUMO+8 (27%) HOMO $\rightarrow$ LUMO+5 (7%)
3.38	0.1038	HOMO-1 $\rightarrow$ LUMO+4 (58%) HOMO $\rightarrow$ LUMO+8 (16%)
3.39	0.1559	HOMO-1 $\rightarrow$ LUMO+4 (36%) HOMO $\rightarrow$ LUMO+8 (14%) HOMO-2 $\rightarrow$ LUMO+1 (9%) HOMO-4 $\rightarrow$ LUMO (8%) HOMO $\rightarrow$ LUMO+2 (5%)
3.84	0.048	HOMO-11 $\rightarrow$ LUMO (25%) HOMO-6 $\rightarrow$ LUMO+4 (14%) HOMO-4 $\rightarrow$ LUMO+7 (11%) HOMO-1 $\rightarrow$ LUMO+7 (8%) HOMO-1 $\rightarrow$ LUMO+6 (6%)
3.86	0.0434	HOMO-6 $\rightarrow$ LUMO+4 (26%) HOMO-5 $\rightarrow$ LUMO+5 (17%) HOMO-4 $\rightarrow$ LUMO+4 (15%) HOMO-6 $\rightarrow$ LUMO+5 (7%)



**Figure S15** Frontier orbitals involved in the significant UV-vis transitions of **2** in the gas phase. The lowest energy transition with significant  $f_{os}$  is HOMO  $\rightarrow$  LUMO+2 which appears to essentially be  $\pi$  to  $\pi^*$  with some POM participation and minimal CT character. Several other transitions show CT towards POM but these are not very strong.

**Table S6** Calculated Gas Phase Electronic Transitions of Compound **3**

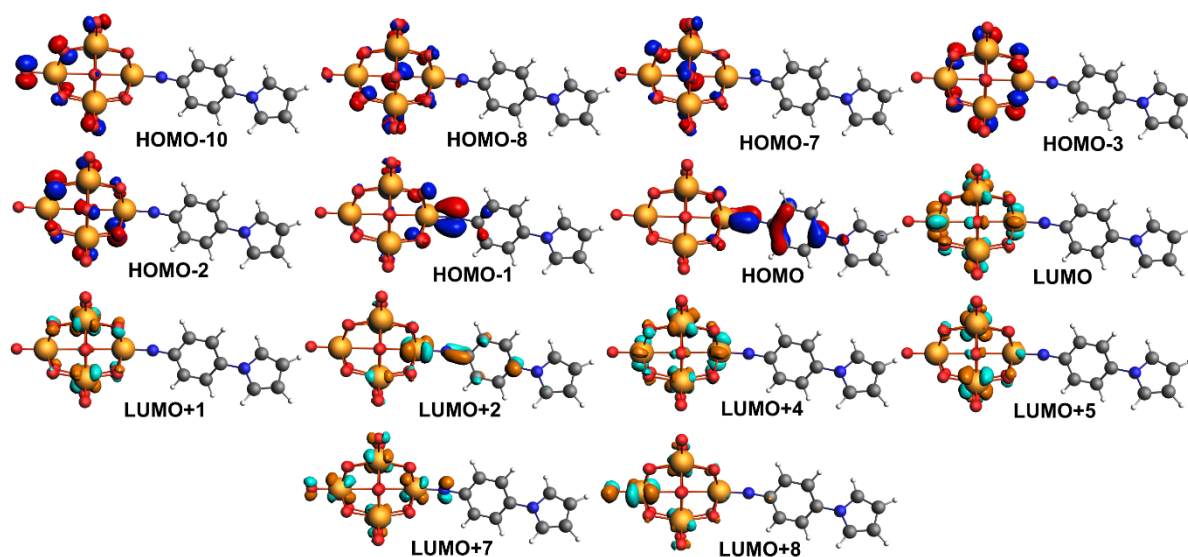
Transition Energy / eV	$f_{os}$	Orbital contributions
2.66	0.2817	HOMO-5 $\rightarrow$ LUMO (57%) HOMO $\rightarrow$ LUMO (39%)
2.80	0.5253	HOMO $\rightarrow$ LUMO (49%) HOMO-5 $\rightarrow$ LUMO (42%)
3.61	0.0216	HOMO-18 $\rightarrow$ LUMO (31%) HOMO-17 $\rightarrow$ LUMO (30%) HOMO-2 $\rightarrow$ LUMO+6 (19%)
3.96	0.0383	HOMO $\rightarrow$ LUMO+13 (23%) HOMO-5 $\rightarrow$ LUMO+6 (12%) HOMO $\rightarrow$ LUMO+12 (9%) HOMO-1 $\rightarrow$ LUMO+10 (9%) HOMO-25 $\rightarrow$ LUMO (9%)



**Figure S16** Frontier orbitals involved in the significant UV-vis transitions of **3** in the gas phase. Much more dipolar character is seen with strong transitions from POM (HOMO-5) and aryl imido group (HOMO) towards the aryl-NO<sub>2</sub> orbitals (LUMO). Higher energy transitions involve a mixture of POM-to-aryl, aryl-to-POM and O-to-Mo CT but are comparatively very weak.

**Table S7** Calculated Gas Phase Electronic Transitions of Compound **4**

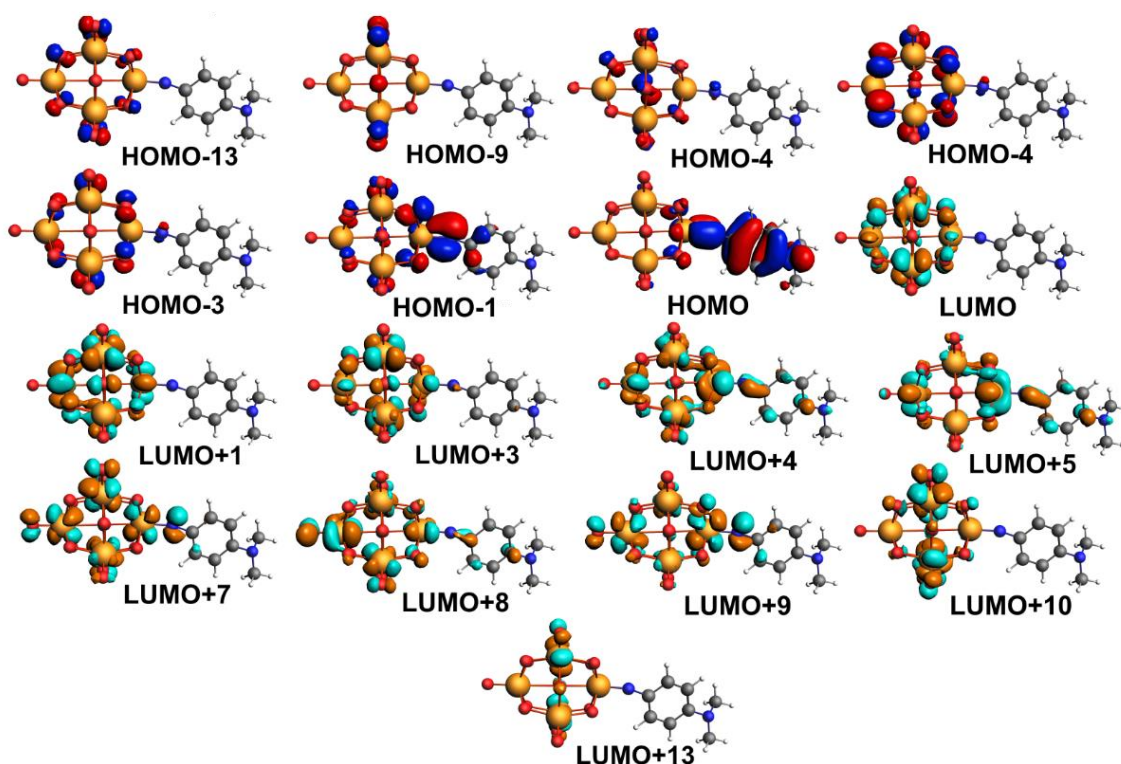
Transition Energy	$f_{os}$	Orbital contributions
3.10 eV	0.3918	HOMO $\rightarrow$ LUMO+2 (56%) HOMO $\rightarrow$ LUMO+8 (21%) HOMO $\rightarrow$ LUMO+5 (13%)
3.43 eV	0.1025	HOMO-1 $\rightarrow$ LUMO+5 (33%) HOMO-3 $\rightarrow$ LUMO+1 (13%) HOMO-1 $\rightarrow$ LUMO+4 (12%) HOMO-2 $\rightarrow$ LUMO+1 (11%) HOMO $\rightarrow$ LUMO+8 (7%)
3.51 eV	0.1077	HOMO $\rightarrow$ LUMO+8 (25%) HOMO-7 $\rightarrow$ LUMO+1 (21%) HOMO-8 $\rightarrow$ LUMO+1 (18%) HOMO-3 $\rightarrow$ LUMO+2 (7%)
3.85	0.0297	HOMO-7 $\rightarrow$ LUMO+4 (28%) HOMO-8 $\rightarrow$ LUMO+4 (23%) HOMO-3 $\rightarrow$ LUMO+7 (11%) HOMO-1 $\rightarrow$ LUMO+7 (10%)
3.87	0.0358	HOMO-8 $\rightarrow$ LUMO (45%) HOMO-1 $\rightarrow$ LUMO+7 (11%) HOMO-10 $\rightarrow$ LUMO+1 (10%)
3.89	0.0327	HOMO-7 $\rightarrow$ LUMO+5 (30%) HOMO-10 $\rightarrow$ LUMO+1 (25%) HOMO-8 $\rightarrow$ LUMO+5 (16%)



**Figure S17** Frontier orbitals involved in the significant UV-vis transitions of **4** in the gas phase. The lowest energy transition with significant  $f_{os}$  (HOMO  $\rightarrow$  LUMO+2) is similar to that of **1** and **2**, essentially being a  $\pi$  to  $\pi^*$  transition that gains some CT character through involvement of the POM orbitals. HOMO $\rightarrow$ LUMO+5 and LUMO+8 involve organic to POM CT but are at quite high energy, as do HOMO-1  $\rightarrow$  LUMO+4/5. There is some CT from the POM to the organic fragment but it is high energy and weak.

**Table S8** Calculated Gas Phase Electronic Transitions of Compound **5**

Transition Energy / eV	$f_{os}$	Orbital contributions
2.92	0.19558	HOMO $\rightarrow$ LUMO+5 (32%) HOMO $\rightarrow$ LUMO+8 (32%) HOMO $\rightarrow$ LUMO+4 (21%) HOMO $\rightarrow$ LUMO+7 (9%)
3.35	0.15206	HOMO $\rightarrow$ LUMO+9 (43%) HOMO $\rightarrow$ LUMO+8 (18%) HOMO-4 $\rightarrow$ LUMO (6%)
3.37	0.12677	HOMO $\rightarrow$ LUMO+9 (20%) HOMO-1 $\rightarrow$ LUMO+4 (18%) HOMO $\rightarrow$ LUMO+10 (14%) HOMO-4 $\rightarrow$ LUMO (11%) HOMO $\rightarrow$ LUMO+8 (11%)
3.43	0.0491	HOMO $\rightarrow$ LUMO+13 (27%) HOMO-6 $\rightarrow$ LUMO (14%) HOMO $\rightarrow$ LUMO+8 (11%) HOMO-4 $\rightarrow$ LUMO (6%)
3.85	0.0312	HOMO-13 $\rightarrow$ LUMO (27%) HOMO-4 $\rightarrow$ LUMO+7 (17%) HOMO-3 $\rightarrow$ LUMO+7 (15%) HOMO-1 $\rightarrow$ LUMO+7 (10%) HOMO-9 $\rightarrow$ LUMO+1 (10%)

**Figure S18** Frontier orbitals involved in the shomoinificant UV-vis transitions of **5** in the gas phase. There is low energy CT from organic to POM (e.g. HOMO $\rightarrow$ LUMO+5/LUMO+8) but no significant CT transitions in the opposite direction.

**Table S9** Calculated Gas Phase Electronic Transitions of Compound **6**

Energy / eV	$f_{os}$	Orbitals
2.46	1.5141	HOMO $\rightarrow$ LUMO (92%)
3.05	0.1602	HOMO $\rightarrow$ LUMO+8 (45%) HOMO-5 $\rightarrow$ LUMO (21%) HOMO $\rightarrow$ LUMO+9 (14%) HOMO $\rightarrow$ LUMO+11 (9%)
3.37	0.1688	HOMO $\rightarrow$ LUMO+11 (26%) HOMO-4 $\rightarrow$ LUMO+2 (21%) HOMO-3 $\rightarrow$ LUMO+3 (10%) HOMO-2 $\rightarrow$ LUMO+3 (6%) HOMO-4 $\rightarrow$ LUMO+3 (5%)
3.438	0.0907	HOMO $\rightarrow$ LUMO+11 (32%) HOMO-4 $\rightarrow$ LUMO+2 (10%) HOMO-4 $\rightarrow$ LUMO+3 (7%) HOMO-8 $\rightarrow$ LUMO (6%) HOMO-3 $\rightarrow$ LUMO+5 (6%)
3.69	0.0742	HOMO-16 $\rightarrow$ LUMO (24%) HOMO-8 $\rightarrow$ LUMO (17%) HOMO-1 $\rightarrow$ LUMO+9 (12%) HOMO-2 $\rightarrow$ LUMO+6 (6%) HOMO-3 $\rightarrow$ LUMO+7 (5%)

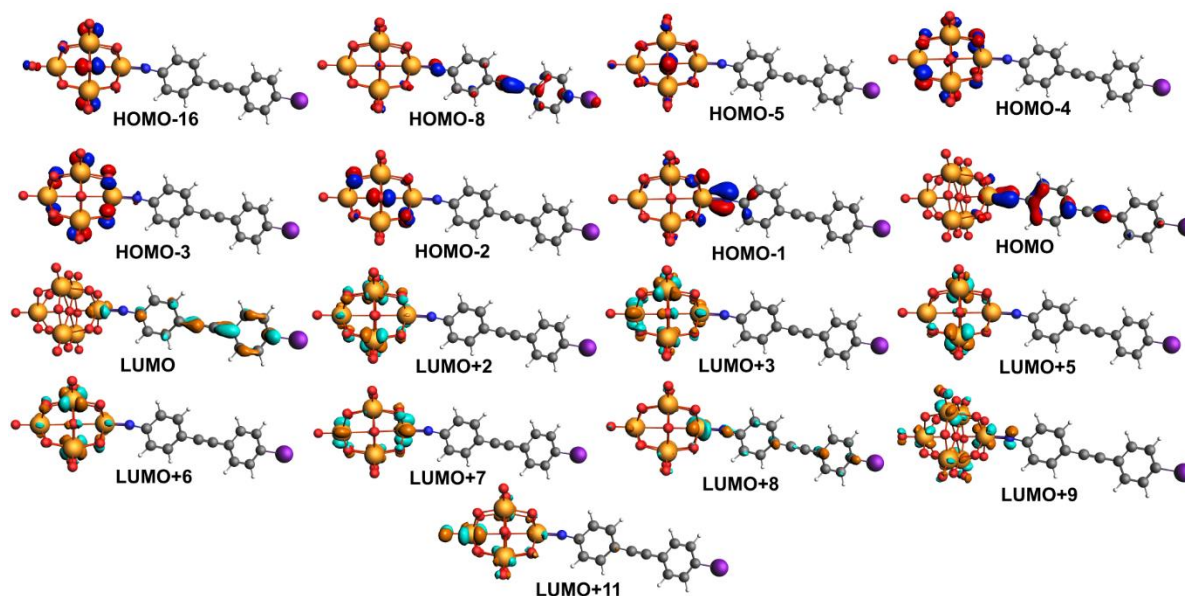


**Figure S19** Frontier orbitals involved in the significant UV-vis transitions of **6** in the gas phase. HOMO to LUMO transition is by far the strongest and involves CT from imido ring to iodo ring. HOMO-5  $\rightarrow$  LUMO, HOMO-8  $\rightarrow$  LUMO, HOMO-16  $\rightarrow$  LUMO also shift electron density in same direction (away from POM). Most transitions at 3.37 eV and above are O-to-Mo CT. HOMO  $\rightarrow$  LUMO+8, +9, +11,; HOMO-1  $\rightarrow$  LUMO+9 oppose dipole of HOMO  $\rightarrow$  LUMO but are much weaker.

**Table S10** Calculated Gas Phase Electronic Transitions of Compound **7**

Energy / eV	$f_{os}$	Orbitals
1.61	0.6919	HOMO → LUMO (69%) HOMO-2 → LUMO (24%)
1.68	0.2455	HOMO-2 → LUMO (75%) HOMO → LUMO (21%)
1.98	0.0388	HOMO-5 → LUMO (95%)
2.61	0.4863	HOMO-16 → LUMO (24%) HOMO-12 → LUMO (22%) HOMO → LUMO+1 (18%) HOMO-11 → LUMO (12%)
2.65	0.2279	HOMO-16 → LUMO (75%) HOMO → LUMO+1 (10%) HOMO-12 → LUMO (5%)
2.81	0.1794	HOMO → LUMO+5 (38%) HOMO-17 → LUMO (34%) HOMO → LUMO+1 (20%)
2.81	0.1273	HOMO → LUMO+5 (61%) HOMO-17 → LUMO (22%) HOMO → LUMO+1 (12%)
3.28	0.0387	HOMO → LUMO+10 (59%) HOMO-5 → LUMO+1 (10%)
3.73	0.0263	HOMO-9 → LUMO+1 (35%) HOMO-3 → LUMO+8 (28%) HOMO-1 → LUMO+8 (14%)

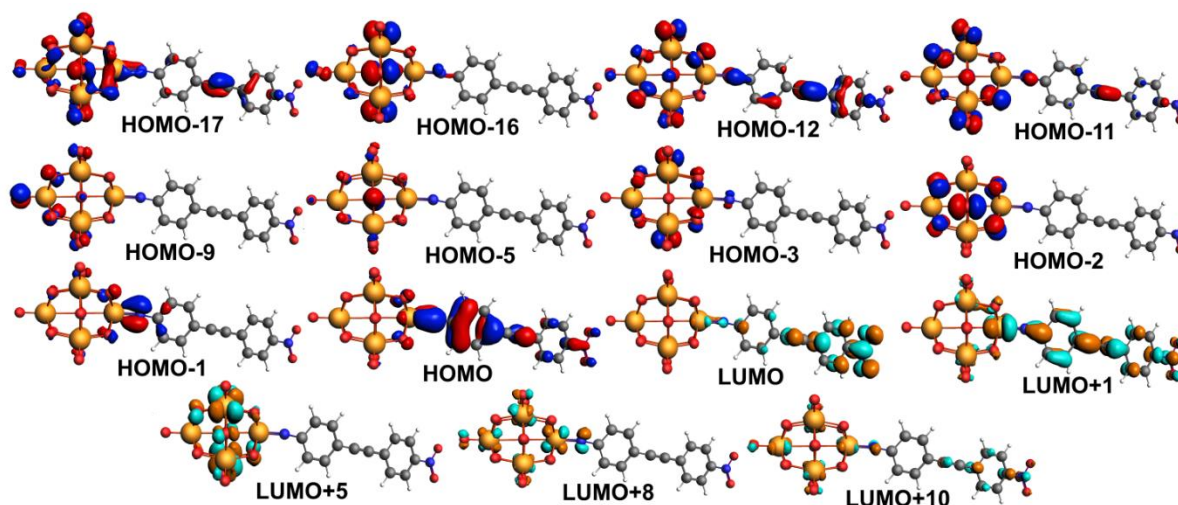


**Figure S20** Frontier orbitals involved in the significant UV-vis transitions of **7** in the gas phase. Again, the HOMO to LUMO transition is strongest, low energy and involves CT away from the POM. HOMO-2, HOMO-16, HOMO-17, HOMO-12 and HOMO-11 to LUMO and HOMO→LUMO+1 all also involve CT towards the nitro group as do several others. HOMO to LUMO+5 however has a significant  $f_{os}$ , is at moderate energy and involves CT towards the POM. Overall, CT to nitro group dominates.

**Table S11** Calculated Gas Phase Electronic Transitions of Compound **8**

Energy / eV	<i>f</i> <sub>os</sub>	Orbitals
2.38	1.4441	HOMO → LUMO (92%)
2.99	0.2524	HOMO → LUMO+6 (38%) HOMO → LUMO+7 (19%) HOMO → LUMO+9 (16%) HOMO → LUMO+10 (6%) HOMO → LUMO+5 (5%)
3.33	0.2976	HOMO → LUMO+10 (62%) HOMO-4 → LUMO+1 (11%) HOMO-4 → LUMO+2 (6%) HOMO-1 → LUMO+5 (5%)
3.71	0.0801	HOMO-1 → LUMO+9 (25%) HOMO-17 → LUMO (14%) HOMO-5 → LUMO+4 (12%) HOMO-8 → LUMO+2 (9%) HOMO → LUMO+12 (6%)

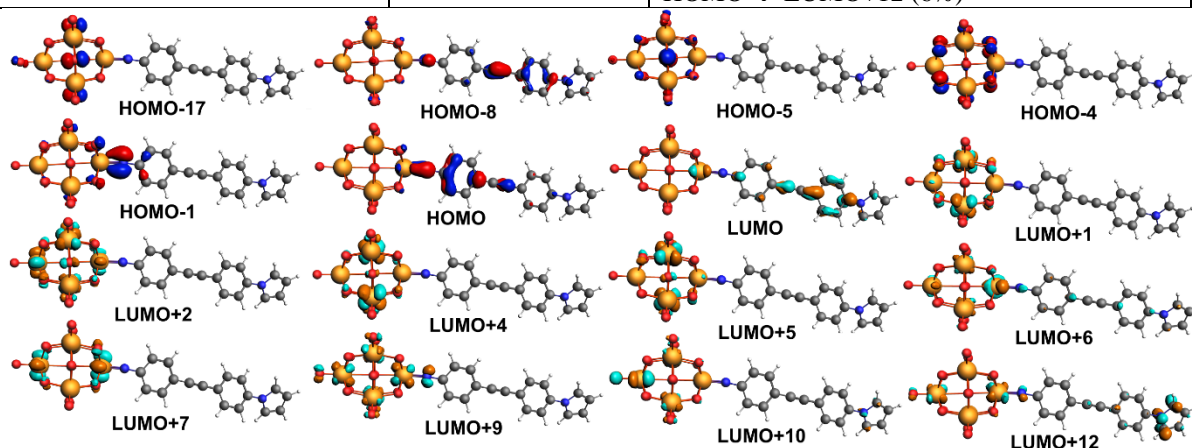


**Figure S21** Frontier orbitals involved in the significant UV-vis transitions of **8** in the gas phase. The lowest energy transition HOMO → LUMO dominates and is similar to in **6** and **7** (CT away from POM in aryl unit). HOMO-17 → LUMO and HOMO → LUMO+12 (both weak and high energy) have CT in same direction. A several significant transitions at intermediate energy (2.99 eV) feature CT to the POM but overall, CT between the two phenyl rings away from POM dominates.

**Table S12** Calculated Gas Phase Electronic Transitions of Compound **9**

Energy / eV	Fos	Orbitals
2.64	0.8468	HOMO → LUMO (77%) HOMO → LUMO+7 (15%)
3.02	0.1404	HOMO → LUMO+9 (39%) HOMO → LUMO+7 (38%) HOMO → LUMO+10 (7%) HOMO → LUMO (5%)
3.04	0.1155	HOMO → LUMO+9 (55%) HOMO → LUMO+7 (26%) HOMO → LUMO+10 (6%)
3.35	0.1056	HOMO → LUMO+10 (29%) HOMO-1 → LUMO+5 (17%) HOMO-1 → LUMO+6 (14%) HOMO-3 → LUMO+2 (12%) HOMO-8 → LUMO (10%) HOMO-2 → LUMO+2 (7%)
3.37	0.2188	HOMO-1 → LUMO+6 (29%) HOMO → LUMO+10 (28%) HOMO-1 → LUMO+5 (14%) HOMO-5 → LUMO+1 (9%) HOMO-5 → LUMO (9%)
3.86	0.0858	HOMO-1 → LUMO+9 (29%) HOMO-4 → LUMO+9 (18%) HOMO-1 → LUMO+11 (9%) HOMO-5 → LUMO+7 (8%) HOMO-8 → LUMO+5 (8%)

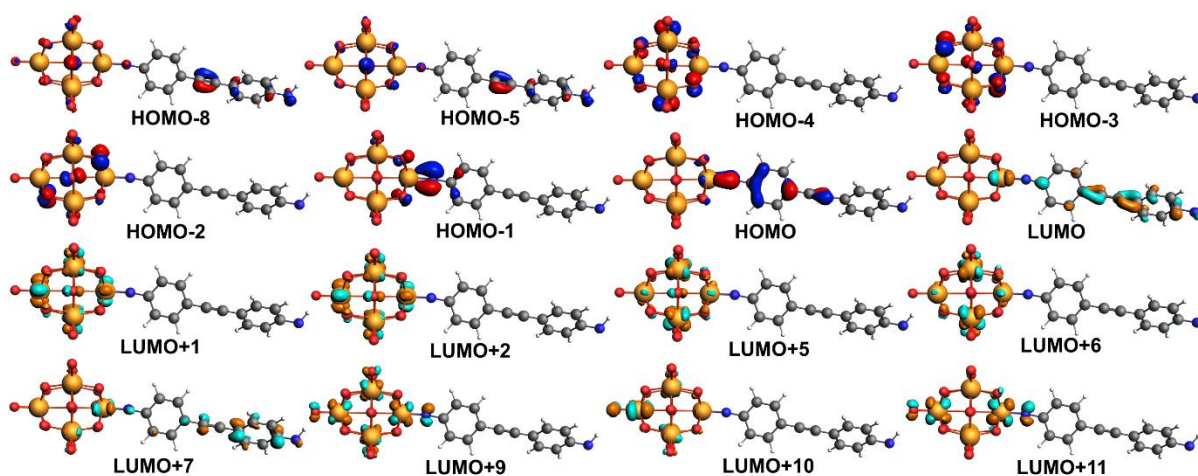


**Figure S22** Frontier orbitals involved in the significant UV-vis transitions of **9** in the gas phase. The lowest energy transition HOMO → LUMO dominates and is similar to in **6** to **8** (CT away from POM in aryl unit). There are several CT processes from the organic group to the POM at higher energy, but despite the -NH<sub>2</sub> donor group these are comparatively weak in the gas phase.

**Table S13** Calculated Gas Phase Electronic Transitions of Compound **10**

Energy / eV	$f_{os}$	Orbitals
2.59	0.1308	HOMO $\rightarrow$ LUMO+3 (87%) HOMO $\rightarrow$ LUMO (8%)
2.62	0.3257	HOMO $\rightarrow$ LUMO+4 (70%) HOMO $\rightarrow$ LUMO (20%) HOMO $\rightarrow$ LUMO+3 (8%)
2.65	0.4660	HOMO $\rightarrow$ LUMO+5 (61%) HOMO $\rightarrow$ LUMO (24%) HOMO $\rightarrow$ LUMO+4 (9%)
2.68	0.8777	HOMO $\rightarrow$ LUMO (41%) HOMO $\rightarrow$ LUMO+5 (37%) HOMO $\rightarrow$ LUMO+4 (18%)
3.30	0.2203	HOMO-5 $\rightarrow$ LUMO (43%) HOMO $\rightarrow$ LUMO+10 (34%) HOMO-6 $\rightarrow$ LUMO (7%)
3.70	0.0159	HOMO-5 $\rightarrow$ LUMO+5 (32%) HOMO-5 $\rightarrow$ LUMO+4 (23%) HOMO-1 $\rightarrow$ LUMO+9 (9%)

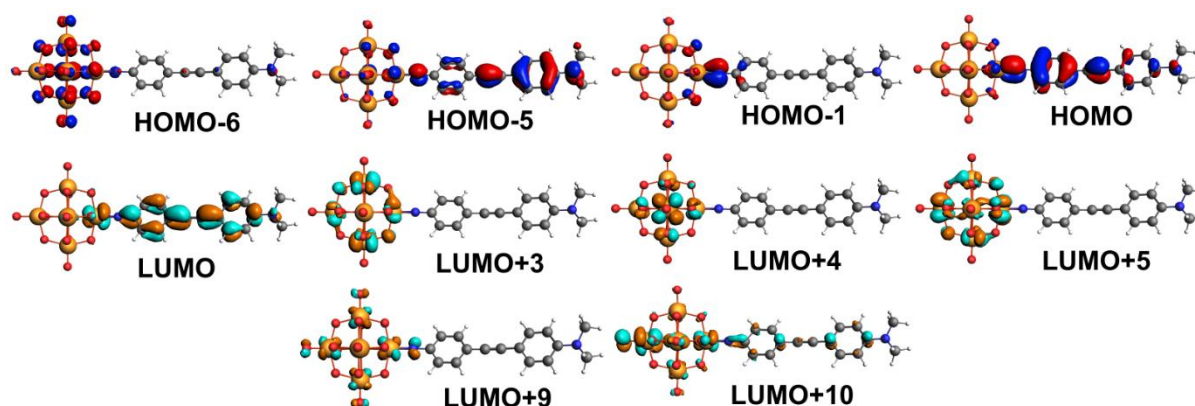


**Figure S23** Frontier orbitals involved in the significant UV-vis transitions of **10** in the gas phase. The lowest energy transition HOMO  $\rightarrow$  LUMO is still the strongest and is similar to in **6** to **9** (CT away from POM in aryl unit). However, it has weakened significantly with the stronger -NMe<sub>2</sub> group while CT transitions towards the POM have become stronger and lower in energy, for example HOMO  $\rightarrow$  LUMO+3, HOMO  $\rightarrow$  LUMO+4, HOMO  $\rightarrow$  LUMO+5, and HOMO  $\rightarrow$  LUMO+10.

## TD-DFT Calculated $\beta$ -values for **1** to **10** in Acetonitrile

**Table S14** Calculated, static  $\beta_{zzz,0}$  tensor components (dominant component along the molecular axis) and orientationally averaged  $\beta_{vec,0}$  values for **1** to **10** in acetonitrile

	$\beta_{zzz,0}^a$	$\beta_{vec,0}^b$
<b>1</b>	398.2	239.9
<b>2</b>	271.5	167.2
<b>3</b>	-78.2	49.8
<b>4</b>	455.1	274.6
<b>5</b>	585.2	356.8
<b>6</b>	1434.3	864
<b>7</b>	-1515.2	922.8
<b>8</b>	1677.2	1009.2
<b>9</b>	1811.7	1088.5
<b>10</b>	4122.3	2480.0
<b>10 twist<sup>a</sup></b>	400.3	237.3

<sup>a</sup>Computation performed on **10** in its crystallographically observed geometry with an 86° twist between the planes of the two phenyl rings, rather than the planar DFT-optimised geometry.

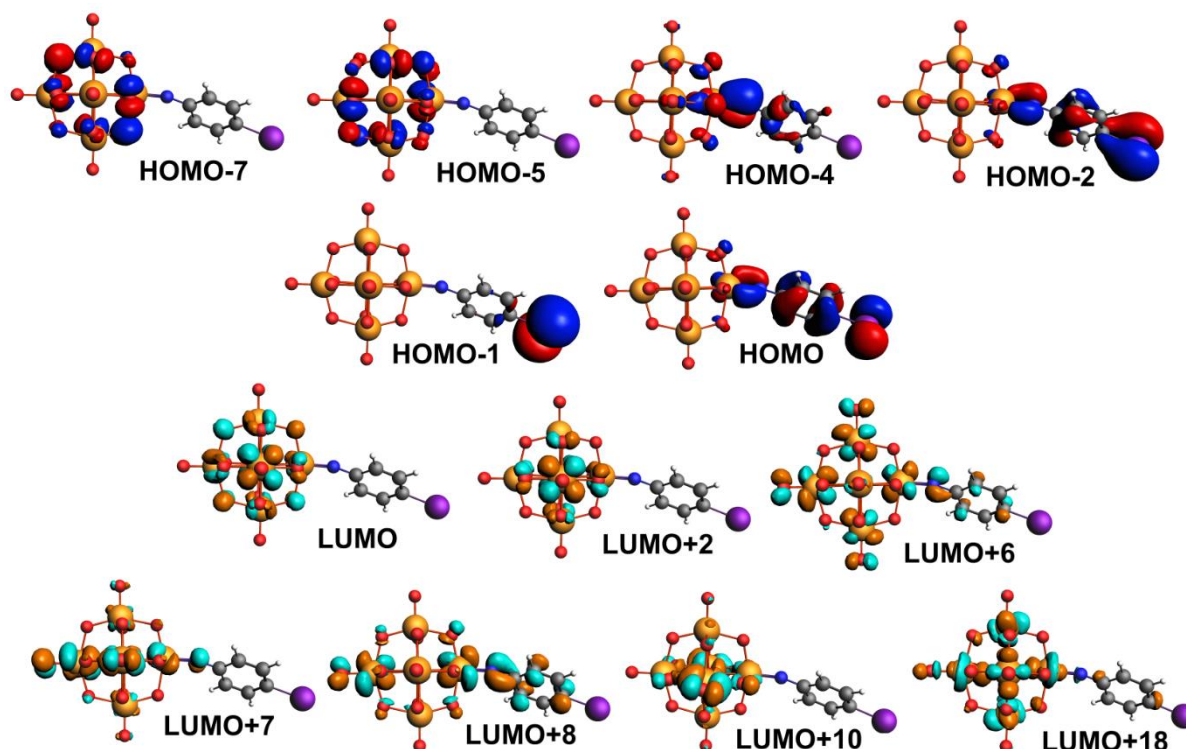
**Table S15** Energies (eV) of the Lowest Vacant POM-based Orbitals of **1** to **10**. The tighter spread of these energies (0.37 eV) in solution, vs gas phase (0.78 eV) is a better fit for the narrow range of POM-based reduction potentials observed experimentally by cyclic voltammetry.

Compound	Gas Phase	Solution
<b>1</b>	-2.877 eV	-8.227 eV
<b>2</b>	-2.882 eV	-8.233 eV
<b>3</b>	-3.308 eV	-8.437 eV
<b>4</b>	-2.848 eV	- 8.177 eV
<b>5</b>	-2.656 eV	-8.107 eV
<b>6</b>	-3.057 eV	-8.180 eV
<b>7</b>	-3.431 eV	-8.28 eV
<b>8</b>	-3.052 eV	-8.183 eV
<b>9</b>	-2.923 eV	-8.119 eV
<b>10</b>	-2.856 eV	-8.065 eV

## TD-DFT Calculated Electronic Transitions in Acetonitrile for 1, 3, 5 and 10

Table S16 Calculated Electronic Transitions of Compound 1 in Acetonitrile solution

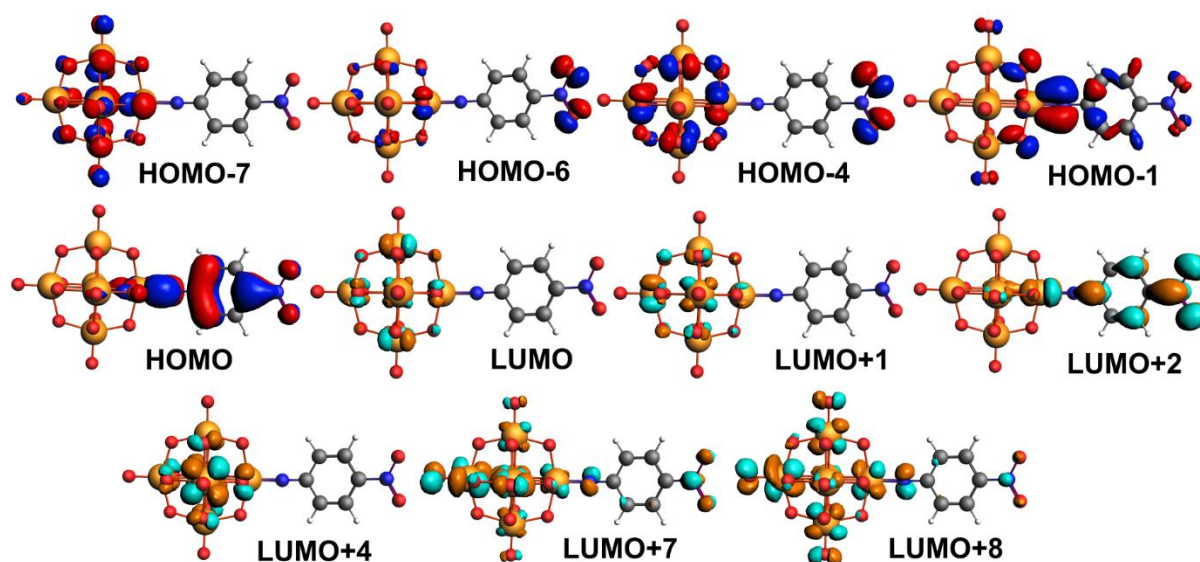
Transition Energy / eV	$f_{os}$	Orbital contributions
2.08	0.1209	HOMO $\rightarrow$ LUMO+6 (71%) HOMO $\rightarrow$ LUMO+7 (25%)
2.12	0.1183	HOMO $\rightarrow$ LUMO+7 (74%) HOMO $\rightarrow$ LUMO+6 (23%)
2.75	0.4660	HOMO $\rightarrow$ LUMO+8 (53%) HOMO-1 $\rightarrow$ LUMO+7 (19%) HOMO $\rightarrow$ LUMO+10 (9%)
3.46	0.1019	HOMO-4 $\rightarrow$ LUMO+7 (66%) HOMO-7 $\rightarrow$ LUMO (6%) HOMO-5 $\rightarrow$ LUMO+2 (6%)
3.72	0.1283	HOMO-2 $\rightarrow$ LUMO+8 (42%) HOMO $\rightarrow$ LUMO+18 (18%) HOMO-2 $\rightarrow$ LUMO+10 (13%)



**Figure S24** Frontier orbitals involved in the significant UV-vis transitions of **1** in solution. Charge transfer in the lowest energy transitions is now strongly towards POM based orbitals of LUMO+6 and LUMO+7. Many of the higher energy transitions are also from the organic group towards the POM, and there are no significant transitions that transfer charge from POM to organic.

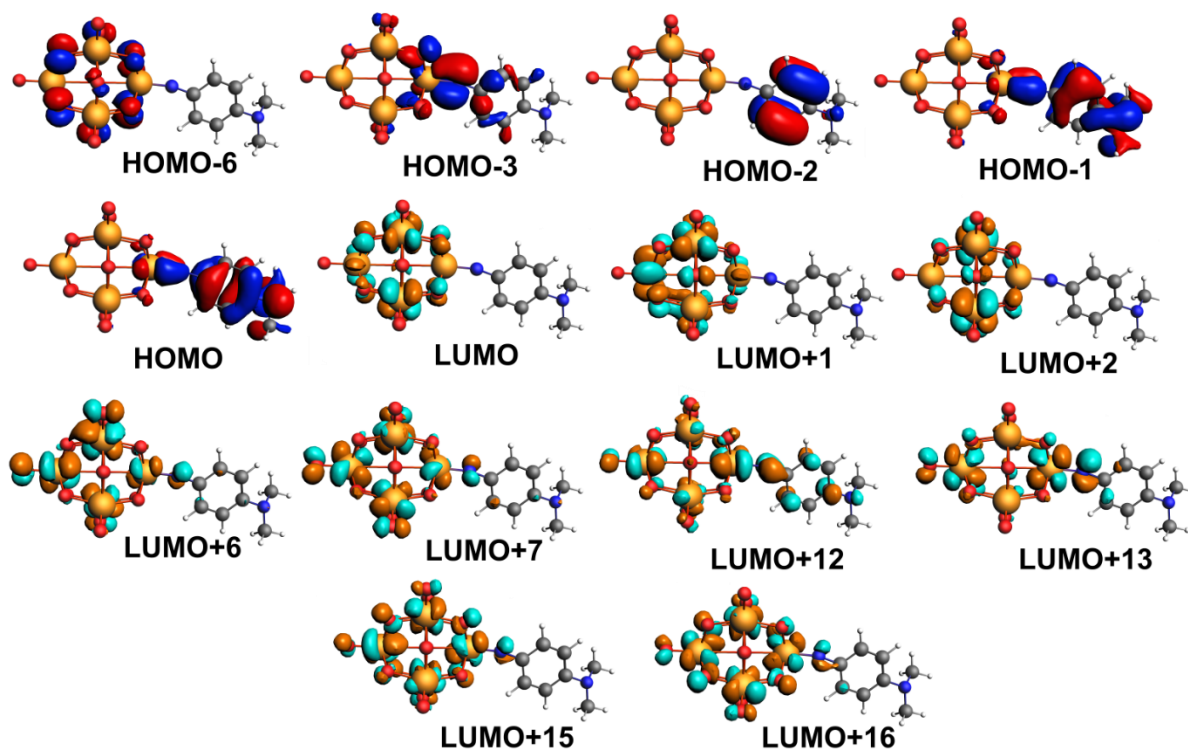
**Table S17** Calculated Electronic Transitions of Compound **3** in Acetonitrile Solution

Transition Energy / eV	$f_{os}$	Orbital contributions
2.44	1.0711	HOMO $\rightarrow$ LUMO+2 (83%) HOMO $\rightarrow$ LUMO+7 (7%)
2.79	0.2142	HOMO $\rightarrow$ LUMO+7 (61%) HOMO $\rightarrow$ LUMO+8 (24%) HOMO $\rightarrow$ LUMO+2 (9%)
3.38	0.0392	HOMO-4 $\rightarrow$ LUMO+1 (36%) HOMO-4 $\rightarrow$ LUMO (14%) HOMO-6 $\rightarrow$ LUMO (10%) HOMO-6 $\rightarrow$ LUMO+1 (9%)
3.53	0.0832	HOMO-7 $\rightarrow$ LUMO+2 (43%) HOMO-1 $\rightarrow$ LUMO+8 (21%) HOMO-1 $\rightarrow$ LUMO+7 (7%) HOMO-4 $\rightarrow$ LUMO+4 (5%)

**Figure S25** Frontier orbitals involved in the significant UV-vis transitions of **3** in solution. Solvation lowers energy of POM orbitals and makes them a significant acceptor. However, the strongest transition (HOMO-to-LUMO+2) still involves CT to the nitro group.

**Table S18** Calculated Electronic Transitions of Compound **5** in Acetonitrile solution

Transition Energy / eV	$f_{os}$	Orbital contributions
1.74	0.1576	HOMO $\rightarrow$ LUMO+7 (80%) HOMO $\rightarrow$ LUMO+6 (16%)
2.50	0.4357	HOMO $\rightarrow$ LUMO+12 (50%) HOMO-1 $\rightarrow$ LUMO+2 (18%) HOMO $\rightarrow$ LUMO+15 (6%) HOMO $\rightarrow$ LUMO+16 (6%)
2.88	0.2491	HOMO $\rightarrow$ LUMO+16 (56%) HOMO-3 $\rightarrow$ LUMO+2 (17%) HOMO $\rightarrow$ LUMO+15 (13%) HOMO $\rightarrow$ LUMO+12 (7%)
3.42	0.0997	HOMO-3 $\rightarrow$ LUMO+7 (26%) HOMO-6 $\rightarrow$ LUMO (23%) HOMO-3 $\rightarrow$ LUMO+6 (18%) HOMO-6 $\rightarrow$ LUMO+1 (8%)
3.72	0.0777	HOMO-1 $\rightarrow$ LUMO+13 (35%) HOMO-1 $\rightarrow$ LUMO+12 (32%) HOMO-2 $\rightarrow$ LUMO+12 (12%)

**Figure S26** Frontier orbitals involved in the significant UV-vis transitions of **5** in solution. Charge transfer towards the POM becomes stronger, and lower energy than in the gas phase.

**Table S19** Calculated Electronic Transitions of Compound **10** in Acetonitrile Solution

Energy / eV	$f_{os}$	Orbital contributions
1.37	0.3185	HOMO → LUMO+6 (84%) HOMO → LUMO+7 (14%)
1.40	0.1078	HOMO → LUMO+7 (86%) HOMO → LUMO+6 (13%)
1.88	0.1695	HOMO → LUMO+9 (63%) HOMO → LUMO+8 (31%)
1.89	0.2182	HOMO → LUMO+9 (32%) HOMO → LUMO+8 (31%) HOMO-1 → LUMO+3 (13%) HOMO → LUMO+11 (11%) HOMO → LUMO+10 (11%)
1.94	0.2408	HOMO → LUMO+11 (64%) HOMO → LUMO+8 (19%) HOMO → LUMO (8%)
2.30	0.0973	HOMO-1 → LUMO+6 (37%) HOMO-1 → LUMO+7 (36%) HOMO → LUMO+14 (22%)
2.88	0.2383	HOMO-5 → LUMO+2 (57%) HOMO-1 → LUMO+8 (23%) HOMO-1 → LUMO+11 (6%)
2.89	0.3472	HOMO-1 → LUMO+8 (33%) HOMO-6 → LUMO+2 (23%) HOMO-5 → LUMO+2 (22%) HOMO-1 → LUMO+11 (9%)
3.34	0.2659	HOMO-1 → LUMO+15 (74%) HOMO → LUMO+21 (5%) HOMO-7 → LUMO+1 (4%)
3.50	0.1845	HOMO → LUMO+21 (26%) HOMO → LUMO+20 (25%) HOMO-1 → LUMO+15 (6%) HOMO-7 → LUMO+3 (6%) HOMO-6 → LUMO+8 (6%)

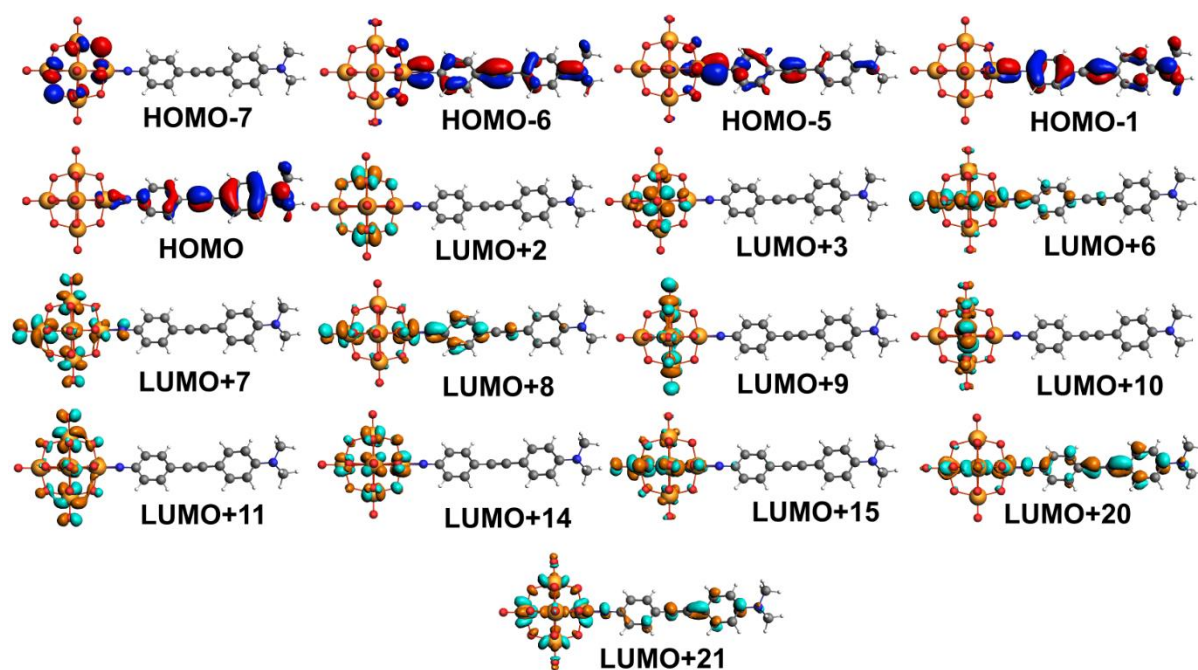
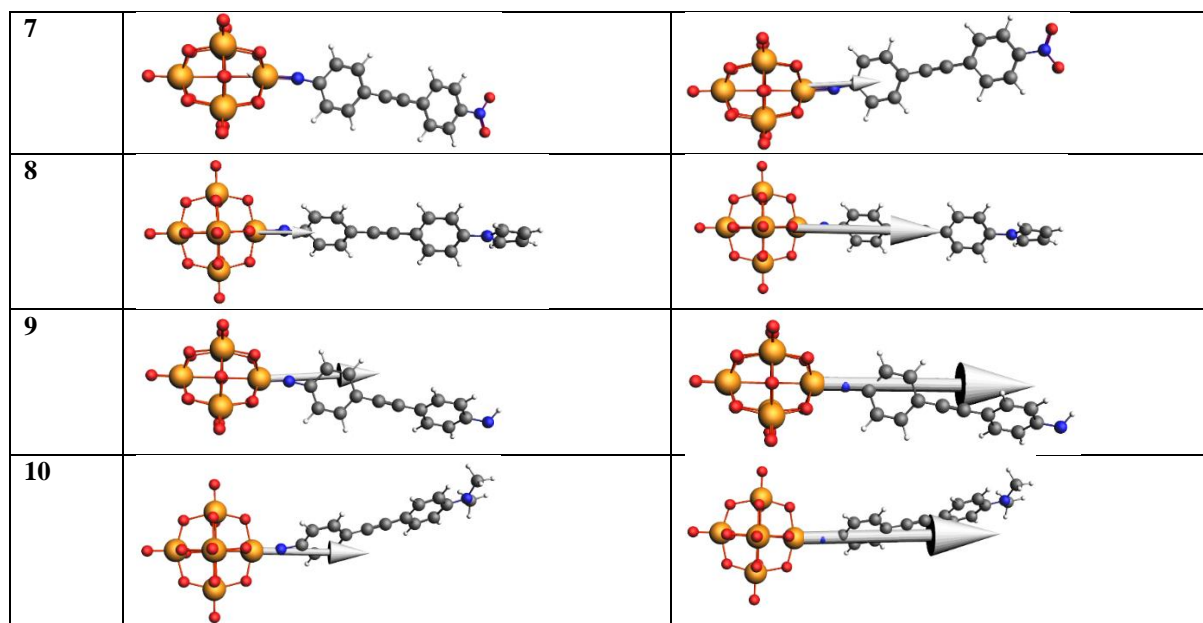


**Figure S27** Frontier orbitals involved in the significant UV-vis transitions of **10** in acetonitrile. The strongest and lowest energy transitions are now all CT from organic unit to POM. It can be assumed that a similar strengthening of CT to the POM occurs in **6** to **9** in solution.

**Table S20** Pictorially represented ground state dipoles **1** to **10** in the gas phase and in acetonitrile

Anion	Gas Phase	Acetonitrile Solution
<b>1</b>		
<b>2</b>		
<b>3</b>		
<b>4</b>		
<b>5</b>		
<b>6</b>		



## References

1. Armarego, W. L. F.; Chai, C. L. L. *Purification of laboratory chemicals*; 6th ed.; Elsevier/Butterworth-Heinemann: Amsterdam; Boston, **2009**.
2. Klemperer, W. G. Tetrabutylammonium Isopolyoxometalates. *Inorg. Synth.* **1990**, *27*, 74.
3. Deng, H.-J.; Fang, Y.-J.; Chen, G.-W.; Liu, M.-C.; Wu, H.-Y.; Chen, J.-X. Copper-catalyzed Clauson-Kass pyrroles synthesis in aqueous media. *Appl. Organometallic Chem.* **2012**, *26*, 164.
4. Al-Yasari, A.; Van Steerteghem, N.; El Moll, H.; Clays, K.; Fielden, J. Donor-acceptor organo-imido polyoxometalates: high transparency, high activity redox-active NLO chromophores. *Dalton Trans.* **2016**, *45*, 2818.
5. Mongin, O.; Gossauer, A. Synthesis of Nanometer-sized Homo and Heteroorganometallic Tripodaphyrins. *Tetrahedron* **1997**, *53*, 6835.
6. Matt, B.; Renaudineau, S.; Chamoreau, L. M.; Afonso, C.; Izzet, G.; Proust, A. Hybrid Polyoxometalates: Keggin and Dawson Silyl Derivatives as Versatile Platforms. *J. Org. Chem.* **2011**, *76*, 3107.
7. Si, G.; Wang, W.-G.; Wang, H.-Y.; Tung, C.-H.; Wu, L.-Z. Facile Synthesis and Functionality-Dependent Electrochemistry of Fe-Only Hydrogenase Mimics. *Inorg. Chem.* **2008**, *47*, 8101.
8. *CrysAlisPro* (Version 1.171.36.21), Agilent Technologies, Inc.; Santa Clara: CA, United States, **2012**.
9. *CrystalClear-SM Expert* (Version 3.1 b27), Rigaku Corporation; Tokyo: Japan, **2013**.
10. Sheldrick, G. M. *SHELXS-2014*, Programs for Crystal Structure Analysis (Release 2014-7); University of Göttingen: Göttingen, Germany, **2014**.
11. Altomare, A.; Cascarano, G.; Giacovazzo, C.; Guagliardi, A.; Burla, M. C.; Polidori, G.; Camalli, M. *SIR92* – a program for automatic solution of crystal structures by direct methods. *J. Appl. Cryst.* **1994**, *27*, 435.
12. Farrugia, L. J. *WinGX* suite for small-molecule single-crystal crystallography. *J. Appl. Cryst.* **1999**, *32*, 837.
13. Sheldrick, G. M. *SHELXL-2014*, Programs for Crystal Structure Analysis (Release 2014-7); University of Göttingen: Göttingen, Germany, **2014**.
14. Farrugia, L. J. *ORTEP-3* for Windows – a version of *ORTEP-III* with a Graphical User Interface (GUI) *J. Appl. Cryst.* **1997**, *30*, 565.
15. CCDC, *Mercury 3.8*, Cambridge Crystallographic Data Centre, Cambridge, UK, **2016**.

16. Spek, A. L. Structure validation in chemical crystallography. *Acta. Cryst.* **2009**, *D65*, 148.
17. (a) Strong, J. B.; Yap, G. P. A.; Ostrander, R.; Liable-Sands, L. M.; Rheingold, A. L.; Thouvenot, R.; Gouzerh, P.; Maatta, E. A. A New Class of Functionalized Polyoxometalates: Synthetic, Structural, Spectroscopic, and Electrochemical Studies of Organoimido Derivatives of  $[\text{Mo}_6\text{O}_{19}]^{2-}$ . *J. Am. Chem. Soc.* **2000**, *122*, 639. (b) Xu, B.; Wei, Y.; Barnes, C. L.; Peng, Z. Hybrid Molecular Materials Based on Covalently Linked Inorganic Polyoxometalates and Organic Conjugated Systems. *Angew. Chem. Int. Ed.* **2001**, *40*, 2290.
18. (a) te Velde, G.; Bickelhaupt, F. M.; Baerends, E. J.; Fonseca Guerra, C.; van Gisbergen, S. J. A.; Snijders, J. G.; Ziegler, T. Chemistry with ADF. *J. Comput. Chem.* **2001**, *22*, 931. (b) Fonseca Guerra, C.; Snijders, J. G.; Te Velde, G.; Baerends, E. Towards an order-N DFT method. *J. Theor. Chem. Acc.* **1998**, *99*, 391. (c) ADF2014.10, SCM, Theoretical Chemistry, Vrije Universiteit, Amsterdam, The Netherlands, <http://www.scm.com>.
19. van Lenthe, E.; Baerends, E. J.; Snijders, J. G. Relativistic regular two-component Hamiltonians. *J. Chem. Phys.* **1993**, *99*, 4597.
20. Becke, A. D. Density-functional exchange-energy approximation with correct asymptotic behavior. *Phys. Rev. A* **1988**, *38*, 3098.
21. Perdew, J. P. Density-functional approximation for the correlation energy of the inhomogeneous electron gas. *Phys. Rev. B* **1986**, *33*, 8822.
22. van Gisbergen, S. J. A.; Snijders, J. G.; Baerends, E. Implementation of time-dependent density functional response equations. *Comput. Phys. Commun.* **1999**, *118*, 119.
- 23 (a) Gritsenko, O. V.; Schipper, P. R. T.; Baerends, E. J. Approximation of the exchange-correlation Kohn-Sham potential with a statistical average of different orbital model potentials. *Chem. Phys. Lett.* **1999**, *302*, 199; (b) Schipper, P. R. T.; Gritsenko, O. V.; van Gisbergen, S. J. A.; Baerends, E. J. Molecular calculations of excitation energies and (hyper) polarizabilities with a statistical average of orbital model exchange-correlation potentials. *J. Chem. Phys.* **2000**, *112*, 1344.
24. (a) Yan, L.; Yang, G.; Guan, W.; Su, Z.; Wang, R. Density Functional Theory Study on the First Hyperpolarizabilities of Organoimido Derivatives of Hexamolybdates. *J. Phys. Chem. B* **2005**, *109*, 22332. (b) Yang, G.; Guan, W.; Yan, L.; Su, Z.; Xu, L.; Wang, E. B. Theoretical Study on the Electronic Spectrum and the Origin of Remarkably Large Third-Order Nonlinear Optical Properties of Organoimide Derivatives of Hexamolybdates. *J. Phys. Chem. B* **2006**, *110*, 23092. (c) Janjua, M. R. S. A.; Amin, M.; Ali, M.; Bashir, B.; Khan, M. U.; Iqbal, M. A.; Guan, W.; Yan, L.; Su, Z.–M. A DFT Study on The Two-Dimensional Second-Order Nonlinear Optical (NLO) Response of Terpyridine-Substituted Hexamolybdates: Physical Insight on 2D Inorganic–Organic Hybrid Functional Materials. *Eur. J. Inorg. Chem.* **2012**, 705. (d) Janjua, M. R. S. A.; Khan, M. U.; Bashir,

B.; Iqbal, M. A.; Song, Y.; Naqvi, S. A. R.; Khan, Z. A. Effect of  $\pi$ -conjugation spacer on the first hyperpolarizabilities of polymeric chain containing polyoxometalate cluster as a side-chain pendant: A DFT study. *Comp. Theor. Chem.*, **2012**, 994, 34.